

EXISTENCE THEOREMS FOR THIN INFLATED WRINKLED MEMBRANES SUBJECTED TO A HYDROSTATIC PRESSURE

Frank Baginski
George Washington University
Washington, DC 20052
baginski@gwu.edu

Michael Barg
George Washington University
Washington, DC 20052
mc_barg@gwu.edu

William Collier
5912 Seventeenth Street NW,
Washington, DC 20011
wcollier@csc.com

July 31, 2018

Abstract

In this paper, we establish rigorous existence theorems for a mathematical model of a thin inflated wrinkled membrane that is subjected to a shape dependent hydrostatic pressure load. We are motivated by the problem of determining the equilibrium shape of a strained high altitude large scientific balloon. This problem has a number of unique features. The balloon is very thin (20-30 μm), especially when compared with its diameter (over 100 meters). Unlike a standard membrane, the balloon is unable to support compressive stresses and will wrinkle or form folds of excess material. Our approach can be adapted to a wide variety of inflatable membranes, but we will focus on two types of high altitude balloons, a zero-pressure natural shape balloon and a super-pressure pumpkin shaped balloon. We outline the shape finding process for these two classes of balloon designs, formulate the problem of a strained balloon in an appropriate Sobolev space setting, establish rigorous existence theorems using direct methods in the calculus of variations, and present numerical studies to complement our theoretical results.

1 Introduction

Balloons play an important role in NASA's current scientific investigations, including upper atmosphere research, high energy astrophysics, stratospheric composition, meteorology, and astronomy. With the development of the Ultra Long Duration Balloon (see, e.g., [21]) and the possible uses of balloons in the exploration of planets in our solar system, balloons will play an important role in NASA's future scientific endeavors (see, e.g., [22]). Furthermore, many of the techniques that have been developed for the analysis of balloons can be readily adapted to other light-weight membrane structures, including solar sails, inflatable rovers, aerobots, and gossamer spacecraft.

Large scientific balloons are regularly flown by NASA to carry out research in the stratosphere. With a fully inflated diameter of over 100 meters and a thickness of 20-30 microns, a large scientific

balloon does not behave like a standard inflated membrane. Because the balloon is so thin, it is unable to support compressive stresses and will instead form folds of excess material or wrinkle. Although our theoretical results could be applied to partially inflated balloons with the contact problem handled by constraints, for the numerical simulations considered in this paper, the balloons will be fully or near fully inflated, so wrinkling can occur, but folds cannot form. Because the diameter of a typical balloon is so large in comparison with the thickness of the balloon skin, the problem of a strained large scientific balloon falls outside the realm of typical inflated membranes. For a survey on inflated membranes, including wrinkling, see [23, Chapter V, Section T] and the references therein. To handle wrinkling, one replaces the wrinkled region by a smoothed out pseudo-surface. This can be done via pseudo-constitutive relations as in the work of Stein and Hedgepath [27] where a variable Poisson ratio is introduced. We follow the approach of Pipkin [24] where a “relaxed” strain energy is used to model wrinkling (see also [26]). In addition to wrinkling, the balloon problem is characterized by a number of other features, including large displacements, relatively small strains, and a shape dependent hydrostatic pressure load. Problems in nonlinear elasticity have been well-studied using a variety of methods (see, e.g., [2], [23]), including direct methods in the calculus of variations (see, e.g., [10], [16, Appendix A]), but our existence results for a thin inflated strained large scientific balloon are the first rigorous analytical treatment of this class of membrane problems. Our analytical results affirm the use of numerical models based on optimization, and help explain the efficacy of these types of schemes (see, [5]-[8]).

To date, the workhorse of NASA’s large scientific balloon program has been the zero-pressure natural shape balloon, a design that goes back to the 1950’s (see [1]). In recent years, due to scientists’ demands for long duration mid-latitude balloon flights, a design concept that has come to be known as the pumpkin balloon has been in development. While the design shape of a balloon is a theoretical target which the fully inflated balloon is intended to assume, shape generating models are usually limited to weight and pressure considerations and ignore straining in the film. However, upon inflation, the real balloon envelope responds to the differential pressure and strains. For these reasons, the analysis of an inflated balloon usually is divided into two distinct parts, *shape finding* and *stress analysis*. Shape finding is carried out by the balloon designer. Typically, the fully inflated balloon must maintain a payload at a constant altitude. At float conditions, the shape of the balloon and its volume must be determined. Archimedes’ principle states that the upward force (lift) generated by the lifting gas is equal to the total weight of the balloon system. At equilibrium the lift is equal to the weight of the air displaced by the lifting gas less the weight of the lifting

gas, i.e., $\text{Lift} = g\rho_a\omega_0 - g\rho_g\omega_0$, where g is the gravitational constant, ρ_a is the density of the atmosphere, ρ_g is the density of the lifting gas, and ω_0 is the volume of the gas bubble. ρ_a and ρ_g are functions of altitude, temperature, etc. and are assumed to be known. The specific buoyancy is defined to be $b = g(\rho_a - \rho_g)$. To emphasize that a quantity depends on the design conditions, we add a subscript of ‘ d ’. For example, at float, we have $\text{Lift} = b_d\omega_{0,d}$. We will assume that for other altitudes corresponding to specific buoyancy b and volume ω_0 , the following relation holds

$$b\omega_0 = b_d\omega_{0,d}. \quad (1.1)$$

Note, b is decreasing as a function of altitude, so (1.1) means that volume is increasing as a function of altitude. For example, a balloon with a sea level volume of ω_0 will expand to approximately $300\omega_0$ at 39 kilometers.

The shape finding processes for the two designs discussed here are outlined in Section 2. More detail on shape finding can be found in [4]. A byproduct of the shape finding process is a gore pattern that the manufacturer uses to fabricate the balloon. A gore is a long flat tapered panel of film. The gores are sealed edge-to-edge in such a way that when fully inflated, the complete balloon will assume a shape very similar to the one desired by the balloon designer. The shape of the gore pattern is an important input into the stress analysis.

The second part of the balloon problem involves an analysis of a pressurized elastic membrane. For efficiency, the balloon needs to be as light as possible, yet it must be strong enough to operate safely over its service life. A meaningful stress/strain analysis requires knowledge of certain mechanical properties of the structural elements (e.g., film thickness t , Young’s modulus E , and Poisson’s ratio ν). The membrane is assumed to be made of a linearly elastic isotropic material, and because it is so thin, it is unable to support compressive stresses, and will wrinkle instead. Following the approach of Pipkin [24], we model wrinkling by relaxation of the film strain energy density. Pipkin’s approach was adapted to large scientific balloons by Collier (see, e.g., [15]) and has been used in a number of subsequent papers (see, e.g., [5]-[9]). We assume that the balloon is in a quasi-static steady equilibrium state and because all of the forces on the balloon are conservative, the problem of determining an equilibrium shape can be formulated in terms of a variational principle. This formulation lends itself to theoretical analysis and efficient numerical computation. While the main results of this paper are the existence theorems in Section 4, we also include numerical solutions.

This paper is divided into six sections. In Section 2, we provide some historical background on

mathematical models that are used for the shape finding process. The most common models are derived from the equations for an axisymmetric membrane. We also consider a cyclically symmetric pumpkin balloon. In Section 3, we present a mathematical model for a strained balloon shape. The membrane is modeled as a *nonlinearly elastic membrane shell* (see, [12, Sec. 9.4]). It will be important to distinguish at least three types of balloon configurations: (a) $\Omega \subset \mathbb{R}^2$ - the flat reference configuration or *natural unstrained state*; (b) $\mathcal{S}_0 \subset \mathbb{R}^3$ - an initial curved configuration; (c) $\mathcal{S} \subset \mathbb{R}^3$ - a general configuration (not necessarily in equilibrium). Ω and \mathcal{S}_0 are generated by the shape finding process and \mathcal{S} is generated in the analysis of a strained shape. Our numerical solution process is robust and \mathcal{S}_0 need not be close to the final strained equilibrium state.

Many non-shallow shell theories start with an initial curved reference configuration in equilibrium for some load, and formulate the equilibrium equations in terms of an appropriate displacement field \mathbf{u} from that state corresponding to a load increment. Since the actual balloon is constructed from a number of thin flat tapered panels of film, it is more natural to parameterize our problem in terms of displacement from the flat reference configuration, i.e., $\mathbf{x} : \Omega \rightarrow \mathbb{R}^3$. This is particularly important when considering pumpkin balloons, where *any* curved configuration is necessarily strained and/or wrinkled and there is no obvious equilibrium state \mathcal{S}_0 to begin the solution process. In our approach, we start with a shape \mathcal{S}_0 (usually obtained from the shape finding process), but do not require it to be in equilibrium. Our film strain energy density function W_f is equivalent to the two-dimensional strain energy of Koiter's nonlinearly elastic membrane shell (see, [12, p. 450]). We will assume the balloon is a linearly elastic isotropic material. Our finite element model (FEM) triangulates Ω , then uses piecewise linear elements and constant strain triangles in its implementation. As we will see, closed subspaces of $W^{1,4}(\Omega)$ are the natural setting in which to study the balloon problem. In order for a mathematical model to produce meaningful results for this type of membrane, it is important to take wrinkling into account. This can be accomplished by replacing the usual strain energy density W_f with W_f^* , the quasiconvexification of W_f (see [24]). W_f^* is the largest convex function that does not exceed W_f , and in our case, we are able to calculate an explicit formula for W_f^* . Using the relaxed strain energy density of the membrane, the existence of equilibrium balloon shapes follows from direct methods in the calculus of variations (see, e.g., [16]).

The problem of determining the strained state of a balloon is formulated in Section 3 and existence results are established in Section 4. Variations on the model presented in Section 3 have been used for numerical studies of strained balloons (see, [5]-[9]), however, Section 4 contains the first rigorous

existence results for a model of this type. The tendon model implemented in earlier work (see, e.g., [5]-[9]) treated the tendons as linearly elastic strings whose strain energy was added directly into the total energy of the balloon system. In the present paper, we focus on inextensible tendons, so tendons are included through the use of constraints. Using a very stiff tendon in the models [5]-[9], we obtain results that are consistent with the results presented here. To complement our theoretical results, we will present numerical solutions of strained pumpkin and strained zero-pressure natural shape balloons in Section 5. Our theoretical results apply to asymmetric balloon shapes as well as cyclically symmetric ones, but we will limit our numerical studies here to cyclically symmetric shapes. See [7] for examples of asymmetric balloon shapes. Section 6 includes concluding remarks.

2 The shape finding process

Before moving to the main results of this paper, it is important to have a clear picture of the shape finding process and how it determines a gore pattern. We focus on the axisymmetric zero-pressure natural shape balloon and the cyclically symmetric pumpkin balloon.

2.1 Zero-pressure natural shape balloons

The design shape of a high altitude balloon is normally based on conditions at maximum (i.e., float) altitude. In addition to known quantities such as film weight density per unit area w , suspended payload L , and specific buoyancy b , there are other parameters relevant to the design shape, including the circumferential stress σ_c and a constant differential pressure term p_0 (p_0 is the differential pressure at the base of the balloon, $Z = 0$). The usual force balance analysis for an axisymmetric membrane involving weight and differential pressure (see, e.g., [2, p. 343]) leads to a system of ordinary differential equations

$$\mathbf{0} = \frac{\partial}{\partial s} (R\sigma_m \mathbf{t}) - \sigma_c \mathbf{i} + R\mathbf{f} \quad (2.1)$$

for the generating curve $\mathbf{\Upsilon}(s) = R(s)\mathbf{i} + Z(s)\mathbf{k}$, where $R'(s) = \sin\theta$, $Z'(s) = \cos\theta$, σ_m is the meridional stress, $\mathbf{f} = -p\mathbf{b} - w\mathbf{k}$, $p = bZ + p_0$ is the differential pressure, \mathbf{t} is a unit tangent to the generating curve, \mathbf{b} is the inward normal, and s is arc length of the generating curve. See Figure 1(a). \mathbf{t} makes an angle of θ with \mathbf{k} . The length of the generating curve L_d and $\theta(0) = \theta_0$ are unknown at the start, and are normally found by using a shooting method to solve a nonlinear boundary value problem involving (2.1) and auxiliary conditions (e.g., the total meridional tension in the \mathbf{k} direction at the bottom of the balloon must equal the weight of the suspended payload,

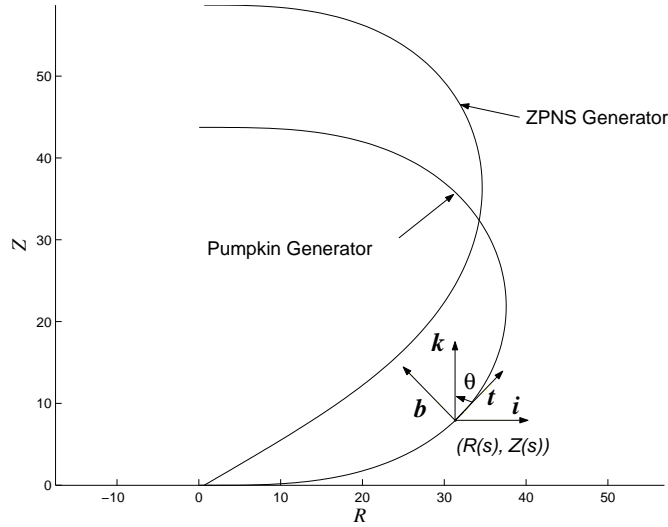


Figure 1: $\Upsilon(s) = R(s)\mathbf{i} + Z(s)\mathbf{k}$; (a) Zero-pressure natural shape gore generator; (b) Pumpkin gore generator Υ . Unit vectors \mathbf{t} , \mathbf{b} , \mathbf{i} , and \mathbf{k} are indicated.

$L/\cos\theta_0 = 2\pi(R\sigma_m)(0)$; zero weight at the top of the balloon implies $R(L_d) = 0$). See [4] for further details.

The model that is used most commonly for applications to large scientific balloons is the *zero pressure natural shape* (ZPNS) model which assumes $p_0 = 0, \sigma_c = 0$ and all tension is carried in the meridional direction. While the assumption of zero hoop stress is clearly violated in a strained float shape, the ZPNS design has proven to be successful for NASA. The original work on high altitude plastic balloons was carried out in the 1950's at the University of Minnesota, where the term natural shape balloon emerged (see, [1]).

The shape finding process for the ZPNS balloon leads to an approximation of the axisymmetric shape by a cyclic shape where a fundamental region $\mathcal{G}_F \subset \mathbb{R}^3$ is taken to be a developable surface (see Figure 2(a)). Thus, there is an isometry that takes \mathcal{G}_F into a plane, from which the “lay-flat” gore pattern G_F is determined. G_F is used by the manufacturer in the construction of the balloon. A typical large zero-pressure natural shape balloon has over 100 gores and it would be hard to distinguish the axisymmetric shape from the cyclically symmetric shape generated by the \mathcal{G}_F . However, in Figure 2(b), we use a small number of gores in order to highlight certain features.

2.2 Pumpkin balloons

In the past, long duration balloon flights took place in regions such as Antarctica where the wind currents are regular and the balloon can circumnavigate the South Pole under the same thermal

conditions for a long period. In 2005, for example, the Cosmic Ray Energetic and Mass Experiment (CREAM) using a ZPNS balloon flew for nearly 42 days, maintaining an altitude between 38 and 39 kilometers for most of its flight. However, at mid-latitudes, a significant amount of ballast must be carried by a ZPNS balloon in order to maintain constant altitude over several diurnal cycles. At night when the temperature of the lifting gas cools, ballast must be dropped, and during the day when the temperature of the gas rises, gas must be vented. Typically, a balloon carries enough ballast for a few of these cycles, restricting the length of a ZPNS mid-latitude flight to no more than a few days. One way to avoid the need to carry significant ballast is to construct a balloon that can contain a sufficient amount of gas to maintain altitude at night and is strong enough to hold the overpressure caused by solar heating during the day. This led to the consideration of a balloon design that has come to be known as the *pumpkin balloon*, a term coined by Smalley in the early 1970's (see, [25]). The pumpkin shape was fore-shadowed by Taylor in his work on parachutes (see [28, Fig. 1]). Currently, NASA's Ultra Long Duration Balloon (ULDB) Program aims to develop a pumpkin balloon that is capable of staying aloft for one hundred days at any latitude. As of the writing of this paper, the ULDB pumpkin has exhibited deployment problems, but these issues are outside the scope of this paper. For more on this topic, see [5]-[8].

The principal behind the pumpkin balloon is to use a light-weight film as a gas barrier and strong reinforcing tendons for pressure confinement and to carry the weight of the balloon system. Roughly speaking, increasing the curvature in the circumferential direction has the effect of transferring most of the load to the tendons. To model the lobing in an ideal pumpkin gore, one can assume a fundamental region \mathcal{G}_F is a subset of a tubular surface. Consequently, the shape \mathcal{G}_F is doubly curved (see Figure 2). If a pumpkin gore is constructed from a flat panel of film, any inflated pumpkin configuration is necessarily strained and/or wrinkled.

Next, we define pumpkin balloons that are analyzed in this paper. We begin with a description of a constant bulge radius pumpkin that is parameterized as a tubular surface. Let $\mathbf{\Upsilon}(s) = R(s)\mathbf{i} + Z(s)\mathbf{k} \in \mathbb{R}^3$ be a planar curve that we call the generator of the pumpkin gore. Arc length measured along the generating curve is denoted by s . See Figure 1(b) for a sketch of a representative $\mathbf{\Upsilon}$ drawn in the RZ -plane. A priori $\mathbf{\Upsilon}$ is unknown, and must be derived from equilibrium conditions. A detailed exposition of the shape finding equations for a pumpkin balloon, including the determination of $\mathbf{\Upsilon}$, is presented in [4]. In the following, we will assume that $\mathbf{\Upsilon}$ is known. The generator is parameterized by s and a prime indicates differentiation with respect to s . Let \mathbf{t} denote the unit tangent and

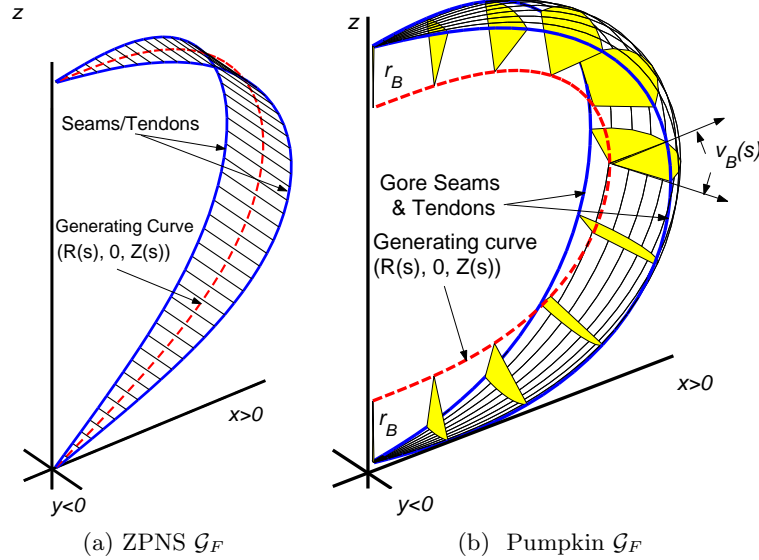


Figure 2: (a) \mathcal{G}_F for a zero-pressure natural shape balloon; (b) Tubular surface \mathcal{G}_F with generating curve Υ and bulge radius r_B .

$\mathbf{b} = \mathbf{t} \times \mathbf{j}$ the inward unit normal of Υ ; $\theta = \theta(s)$ is the angle between \mathbf{t} and \mathbf{k} (see Figure 1(b)). The set $\{\mathbf{b}, \mathbf{t}, \mathbf{j}\}$ gives a right-hand curvilinear basis for \mathbb{R}^3 . The curvature of Υ is denoted by κ where $\Upsilon''(s) = \kappa(s)\mathbf{t}'(s)$. We define a tubular surface with generator Υ and constant radius r_B as follows (see, [17, p. 89]):

$$\mathbf{x}(s, v) = \Upsilon(s) + r_B (\mathbf{j} \sin v - \mathbf{b}(s) \cos v), \quad |v| < v_B(s), \quad 0 < s < L_d, \quad (2.2)$$

where $v_B(s)$ is known from the shape finding process and depends on the number of gores N . See Figure 1 for a typical generating curve and Figure 2(b) for \mathcal{G}_F as determined by the shape-finding process for a pumpkin balloon based on a tubular surface model.

We assume that the pumpkin gore \mathcal{G}_F is situated symmetrically with respect to the $y = 0$ plane and interior to the wedge defined by the half-planes $y = \pm \tan(\pi/N)x$ where N is the number of gores and $x \geq 0$. We will refer to r_B as the *bulge radius* of the pumpkin gore. The curve traced by $v \rightarrow \Upsilon(s) + r_B(\mathbf{j} \sin v - \mathbf{b}(s) \cos v)$ is a circle lying in the plane with normal $\mathbf{t}(s)$. By construction, the length of the circular arc that is formed in the pumpkin gore is $2r_B v_B(s)$ (see Figure 2(b)). We call $v_B(s)$ the *bulge angle*. For large balloons with a large number of gores, $0 < r_B \kappa(s) \ll 1$, but in Figure 2(b), we used a small number of gores in order to highlight certain features. A typical large pumpkin balloon has over 200 gores, yet the lobing in a fully deployed pumpkin is clear to see (see [8, Figure 2(a)]). We define the theoretical three-dimensional pumpkin gore \mathcal{G}_F to be

$$\mathcal{G}_F = \{(x, y, z) = \mathbf{x}(s, v), \quad -v_B(s) < v < v_B(s), \quad 0 < s < L_d\}.$$

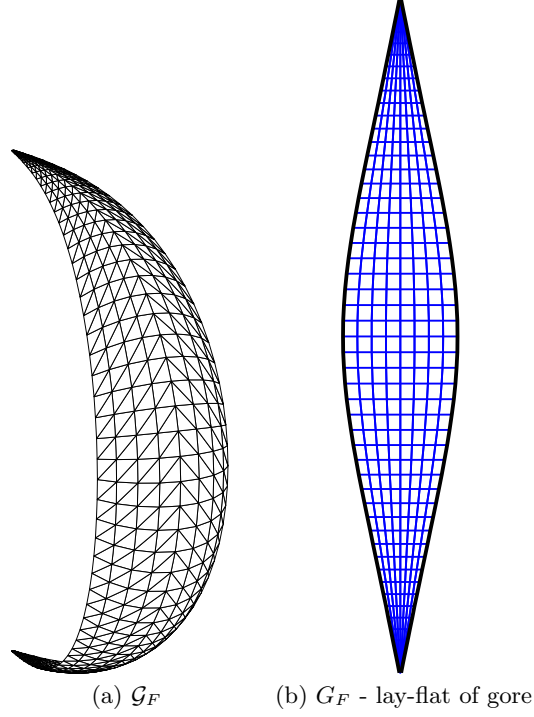


Figure 3: (a) \mathcal{G}_F -initial three dimensional gore configuration; (b) $\Omega_F = G_F$ - usual lay flat component for one pumpkin gore.

A complete shape \mathcal{S}_0 has cyclic symmetry and is made of N copies of \mathcal{G}_F . Note that the length of the centerline of \mathcal{G}_F is

$$L_c = \int_0^{L_d} (1 + r_B \kappa(s)) ds.$$

Normally, the length of a tendon is taken to be

$$L_t = \int_0^{L_d} (1 + r_B \kappa(s) \cos(v_B(s))) ds.$$

Corresponding to $\mathcal{G}_F \subset \mathbb{R}^3$ is the lay-flat configuration $G_F \subset \mathbb{R}^2$ shown in Figure 3(b). The respective centerlines of \mathcal{G}_F and G_F are isometric. The length of a rib (i.e., a circular arc) in the spine of \mathcal{G}_F is $2r_B v_B(s)$ and this is the same as the length of a corresponding segment orthogonal to the centerline of G_F . It follows that L_s , the corresponding edge length of the nominal lay-flat pattern G_F , is longer than the tendon length L_t . For the pumpkin example considered in Section 5, $L_s = 1.005L_t$. A tendon is normally encased in a sleeve that is sealed along the length of a gore seam. To accommodate the lack-of-fit, the sleeve is gathered first. The tendon is tacked to the gathered sleeve at a number of locations. The amount of gathering is not uniform. Maximum gathering takes place near the equator, and decreases as one gets closer to the central axis of the balloon. The smoothed out sleeve and the edges of two adjacent gores are heat sealed together to form one seam.

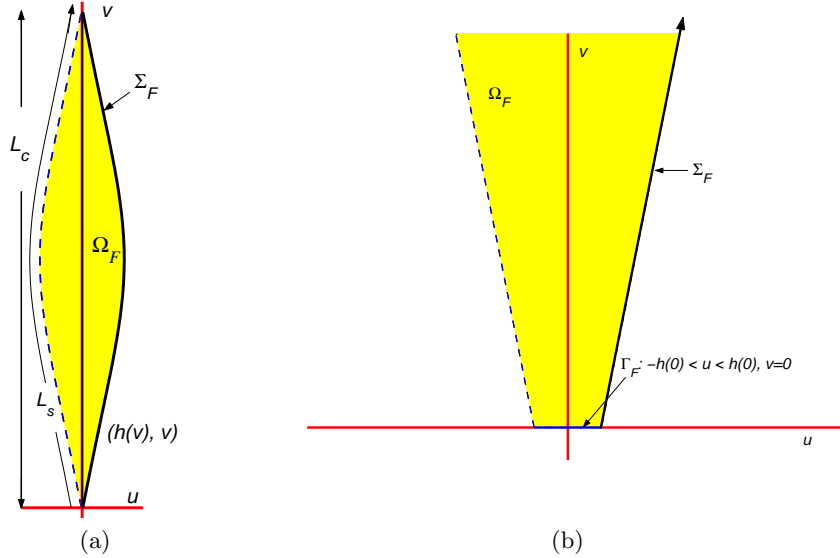


Figure 4: (a) Ω_F ; seam is parametrized by $(h(v), v)$ for $0 < v < L_c$; (b) close up of gore bottom; Γ_F component of Ω_F that will be attached to the end fitting.

The interested reader is referred to [9] and the references therein for a more detailed discussion of tendon-foreshortening and how it affects the film stresses.

3 A model for a strained balloon

In this section, we formulate the problem of a strained balloon and describe the components in our variational principle and related constraints.

3.1 Preliminaries

We first define the reference configuration for a complete balloon. We begin with a discussion of the lay-flat configuration that is obtained from the shape finding process. Let $\Omega_F = G_F$ and let L_c denote the gore length where

$$\Omega_F = \{(u, v) \mid -h(v) < u < h(v), 0 < v < L_c\},$$

and $h(v)$ and L_c are known from the shape-finding process. We can assume that $u = h(v)$ is a $C^{0,1}$ function, so that Ω_F is a $C^{0,1}$ domain. Here, G_F is either a ZPNS gore or a pumpkin gore, but in other applications it may be some other reference configuration. In terms of $h(v)$, the seam length of Ω_F is (see Figure 4(b))

$$L_s = \int_0^{L_c} \sqrt{1 + |h'(v)|^2} dv.$$

Let

$$\begin{aligned}\Gamma_F &= \{(u, v) \mid -h(0) < u < h(0), v = 0\}. \\ \Sigma_F &= \{(u, v) \mid u = h(v), 0 < v < L_c\}.\end{aligned}$$

Let $\Delta > 0$, $\Omega_1 = \Omega_F$, $\Gamma_1 = \Gamma_F$, $\Sigma_1 = \Sigma_F$, and $h_1(v) = h(v)$. We define $h_i(v) = h_{i-1}(v) + \Delta$,

$$\begin{aligned}\Omega_i &= \{(u + (i-1)\Delta, v) \mid (u, v) \in \Omega_1\} \\ \Gamma_i &= \{(u + (i-1)\Delta, v) \mid (u, v) \in \Gamma_1\}, \\ \Sigma_i &= \{(u + (i-1)\Delta, v) \mid (u, v) \in \Sigma_1\},\end{aligned}$$

where $i = 2, \dots, N$. The balloon is constructed from N identical flat gores Ω_i that are sealed edge to edge (in practice, they overlap slightly and $150 \leq N \leq 290$). The right seam of Ω_i is identified with the left seam of Ω_{i+1} . The right seam of Ω_N is identified with the left seam of Ω_1 . With these identifications, we define

$$\Omega = \bigcup_{i=1}^N \Omega_i. \quad (3.1)$$

Remark 1 Due to the slight overlap of the edges of the Ω_i 's as described above, we can think of Ω as defining a two dimensional manifold. For convenience of exposition, we can extend slightly the gore width of the Ω_i 's (call the extended gore $\tilde{\Omega}_i$) so that adjacent local charts overlap (i.e., $\tilde{\Omega}_i \cap \Sigma_i \cap \tilde{\Omega}_{i+1} \neq \emptyset$) and Ω has a manifold structure. Since the overlap is so small in our applications, we treat it as a curve Σ_i . The metric is the usual Euclidean metric on each $\Omega_i \subset \mathbb{R}^2$. Open sets can be defined using this metric with special attention given to points that lie along the seams, i.e., $(u, v) \in \Sigma_i \subset \Omega$. In what follows, we study the balloon problem in a certain Sobolev space. While it is possible to extend the necessary definitions and results such as the Sobolev Embedding Theorems to a manifold setting (see, e.g., [3]), introducing additional notation for this purpose would be cumbersome. Since it only makes sense to consider the differentiability of $\mathbf{x} : \Omega \rightarrow \mathbb{R}^3$ on the Ω_i 's, we adhere to the following conventions. We write $\mathbf{x} \in C^1(\Omega, \mathbb{R}^3)$ to mean $\mathbf{x} \in C^1(\Omega \setminus \cup_{i=1}^N \Sigma_i, \mathbb{R}^3)$. With an appropriate metric defined on Ω , we can consider $\mathbf{x} \in C(\bar{\Omega}, \mathbb{R}^3)$, where the boundary of Ω is $\Gamma = \cup_{i=1}^N \Gamma_i$. With these conventions, we consider mappings $\mathbf{x} \in C^1(\Omega, \mathbb{R}^3) \cap C(\bar{\Omega}, \mathbb{R}^3)$.

Typically, there is an end-plate located at the top and bottom of a balloon, but for simplicity, we assume that a gore comes to a point at the top. Γ corresponds to the bottom end-plate. For ease of exposition, we will assume that the material properties (e.g., Young's modulus, Poisson's ratio, film thickness, etc.) are constant over Ω . We will formulate the equilibrium equations for a complete

balloon, but in practice, we will often assume symmetry in order to reduce the number of degrees of freedom in our numerical model. We assume that $\Omega_F = \Omega_1$ is situated in the uv -plane with its center along the v -axis (see Figure 4).

A deformation mapping for a complete balloon is given by

$$\mathbf{x} : \Omega \rightarrow \mathcal{S} \subset \mathbb{R}^3,$$

where $\mathcal{S} = \mathbf{x}(\Omega)$ represents a balloon configuration and $\mathbf{x} \in \mathcal{D}$ where \mathcal{D} is the set of admissible deformation mappings. Later, we will give a precise definition of \mathcal{D} . Let $\mathcal{S}_0 = \mathbf{x}_0(\Omega)$ denote the initial configuration of the deformed balloon in \mathbb{R}^3 . \mathcal{S}_0 need not be in equilibrium. In our formulation of the problem, the boundary of \mathcal{S} has one component (i.e., $\mathbf{x}_0(\Gamma)$, the part that is attached to the end-plate). For any $\mathbf{x} \in \mathcal{D}$, we require

$$\mathbf{x}(u, v) = \mathbf{x}_0(u, v), \quad (u, v) \in \Gamma.$$

For future reference, we note

$$\boldsymbol{\alpha}_i(v) = \mathbf{x}(h_i(v), v) \text{ for } 0 < v < L_c$$

parameterizes $\boldsymbol{\alpha}|_{\Sigma_i} \subset \mathbb{R}^3$, the deformed seam between Ω_i and Ω_{i+1} for $i = 1, \dots, N-1$. $\boldsymbol{\alpha}_N$ parameterizes the deformed seam between Ω_N and Ω_1 .

We define

$$|\mathbf{x}|_{1,p}^p = |x|_{1,p}^p + |y|_{1,p}^p + |z|_{1,p}^p,$$

where $x(u, v) = \mathbf{x}(u, v) \cdot \mathbf{i}$, $y(u, v) = \mathbf{x}(u, v) \cdot \mathbf{j}$, $z(u, v) = \mathbf{x}(u, v) \cdot \mathbf{k}$,

$$|w|_{1,p}^p = \int_{\Omega} |w|^p dA + \int_{\Omega} |\nabla w|^p dA,$$

$|\nabla \mathbf{x}|^2 = \text{tr}(\nabla \mathbf{x}^T \nabla \mathbf{x}) = |\mathbf{x}_u(u, v)|^2 + |\mathbf{x}_v(u, v)|^2$, and $|\mathbf{x}| = \sqrt{\mathbf{x} \cdot \mathbf{x}}$. ‘ \cdot ’ denotes the usual Euclidean inner product in \mathbb{R}^3 . We will follow the convention that $\mathbf{x}_{,1} = \mathbf{x}_u$ and $\mathbf{x}_{,2} = \mathbf{x}_v$. Let

$$W^{1,p}(\Omega, \mathbb{R}^3) = \{\mathbf{x} : |\mathbf{x}|_{1,p} < \infty\}.$$

Next, we define an admissible deformation mapping.

Definition 1 Let $\mathbf{x}_0(u, v) = x_0(u, v)\mathbf{i} + y_0(u, v)\mathbf{j} + z_0(u, v)\mathbf{k} \in W^{1,p}(\Omega, \mathbb{R}^3)$. An admissible deformation mapping, $\mathbf{x}(u, v) = x(u, v)\mathbf{i} + y(u, v)\mathbf{j} + z(u, v)\mathbf{k}$ is a mapping such that

(a) $\mathbf{x} \in C^1(\Omega) \cap C(\bar{\Omega})$;

(b) $\mathbf{x}(u, v) = \mathbf{x}_0(u, v), (u, v) \in \Gamma$;

(c) $x(u_i, L_c) = y(u_i, L_c) = 0$, for $u_i = (i - 1)\Delta$, $i = 1, 2, \dots, N$;
 $z(u_i, L_c) = z(u_j, L_c)$ for all i, j .

The set of all admissible deformation functions is denoted \mathcal{D} .

In the following, we let

$$X = \left\{ \mathbf{x} = \mathbf{x}_0 + \tilde{\mathbf{x}} \mid \tilde{\mathbf{x}} \in W_0^{1,p}(\Omega, \mathbb{R}^3) \right\}. \quad (3.2)$$

X is the completion of \mathcal{D} with respect to the norm $|\mathbf{x}|_{1,p}$. In our formulation of the balloon problem, $p = 4$ and a solution is $\mathbf{x} = \tilde{\mathbf{x}} + \mathbf{x}_0 \in X$ where $\tilde{\mathbf{x}} \in W_0^{1,4}(\Omega, \mathbb{R}^3)$, and $W_0^{1,4}(\Omega, \mathbb{R}^3)$ is the completion of $C^1(\Omega) \cap C_0(\bar{\Omega})$ with respect to $|\mathbf{x}|_{1,4}$. We will consider closed subspaces of X in the form $X_{\mathbf{g}}$, where $X_{\mathbf{g}}$ is the completion of

$$\mathcal{D}_{\mathbf{g}} = \{ \mathbf{x} \in \mathcal{D} \mid \mathbf{g}(u, v, \mathbf{x}, \nabla \mathbf{x}) \leq \mathbf{0} \}$$

with respect to $|\mathbf{x}|_{1,4}$. $\mathbf{g} = (g_1, g_2, \dots, g_m)$ will incorporate boundary conditions and constraints of a certain type that will ensure $X_{\mathbf{g}}$ is closed.

In the following, we let $\mathbf{x}|_{\mathcal{B}}$ denote the restriction of $\mathbf{x} \in \mathcal{D}$ to $\mathcal{B} \subset \Omega$. Typically, \mathcal{B} will denote a curve in Ω corresponding to the middle of a gore or a gore seam. Since $p = 4$ in our application, the trace of $\mathbf{x} \in X$ for such a set \mathcal{B} is well defined (see [18, p. 257]). In particular, let $\mathbf{x}_k, \mathbf{x} \in X$ and $|\mathbf{x}_k - \mathbf{x}|_{1,4} \rightarrow 0$ and consider g_i 's of the following types:

1. *Global Constraint*

$$g_i(\mathbf{x}) = 0, \quad \text{for } g_i \in C(X, \mathbb{R}). \quad (3.3)$$

From (3.3), we see $\lim_{k \rightarrow \infty} g_i(\mathbf{x}_k) = g_i(\lim_{k \rightarrow \infty} \mathbf{x}_k) = g_i(\mathbf{x})$.

2. *Local Constraint*

$$g_i(\mathbf{x}|_{\mathcal{B}}) \leq 0, \quad \text{for } g_i(\mathbf{x}|_{\mathcal{B}}) \in C(\bar{\mathcal{B}}, \mathbb{R}). \quad (3.4)$$

From (3.4), we see $\lim_{k \rightarrow \infty} g_i(\mathbf{x}_k|_{\mathcal{B}}) = g_i(\lim_{k \rightarrow \infty} \mathbf{x}_k|_{\mathcal{B}}) = g_i(\mathbf{x}|_{\mathcal{B}})$.

We are led to the following.

Lemma 1 *Let $X = \{ \mathbf{x} = \mathbf{x}_0 + \tilde{\mathbf{x}} \mid \tilde{\mathbf{x}} \in W_0^{1,4}(\Omega, \mathbb{R}^3) \}$ and $\mathbf{g} = (g_1, \dots, g_m)$. If g_i satisfies (3.3) or (3.4) for $\mathcal{B} = \mathcal{B}_i \subset \Omega$, $i = 1, 2, \dots, m$, then $X_{\mathbf{g}}$ is a closed subspace, where*

$$X_{\mathbf{g}} = \left\{ \mathbf{x} = \mathbf{x}_0 + \tilde{\mathbf{x}} \mid \tilde{\mathbf{x}} \in W_0^{1,4}(\Omega, \mathbb{R}^3), \mathbf{g}(u, v, \mathbf{x}, \nabla \mathbf{x}) \leq \mathbf{0} \right\}.$$

The proof of Lemma 1 follows directly from the definition of X and (3.3)-(3.4).

We will demonstrate that the components of \mathbf{g} incorporating boundary conditions, symmetry conditions, or tendon constraints satisfy (3.4) and the volume constraint satisfies (3.3). We first consider boundary/symmetry conditions. Tendon constraints are considered in Section 3.3.1 and the volume constraint is considered in Section 3.3.2.

In order to keep the number of degrees of freedom in our numerical model manageable, we use $X_{\mathbf{g}}$ in our simulations. Often, we consider a cyclically symmetric balloon, in which case, we only need to model one-half a gore, i.e., $y = 0$ is a plane of reflectional symmetry and the right deformed seam of Ω_1 must lie in the half plane $y = \tan(\pi/N)x$ with $x \geq 0$. Let us suppose that \mathbf{g} includes boundary conditions for a cyclically symmetric shape with N gores. In this case, there are two constraint boundary conditions. Let $\mathcal{B}_1 = \{(u, v) \mid u = 0, 0 < v < L_c\}$ and $\mathcal{B}_2 = \Sigma_1$,

$$g_1(v, \mathbf{x}(u, v)) = \mathbf{x}(u, v) \cdot \mathbf{j}, \quad (u, v) \in \mathcal{B}_1, \quad (3.5)$$

$$g_2(v, \mathbf{x}(u, v)) = \mathbf{x}(u, v) \cdot (\mathbf{j} - \tan(\pi/N)\mathbf{i}), \quad (u, v) \in \mathcal{B}_2, \quad (3.6)$$

$g_1 = 0$ is the condition that ensures $\mathbf{x}(\Omega_1)$ is symmetric with respect to the $y = 0$ plane and $g_2 = 0$ is the condition that $\mathbf{x}(\Sigma_1)$ lies in the plane $y = \tan(\pi/N)x$. Suppose $\mathbf{x}_k, \mathbf{x} \in X$, $\|\mathbf{x}_k - \mathbf{x}\|_{1,4} \rightarrow 0$, and $\mathbf{g}(\mathbf{x}_k) = \mathbf{0}$ for all k where \mathbf{g} is defined in (3.5)-(3.6). To demonstrate that $X_{\mathbf{g}}$ is closed, we need to show $\mathbf{g}(\mathbf{x}) = \mathbf{0}$, but this is a consequence of the fact that g_1 and g_2 are local constraints in the form (3.4). A similar argument will apply to a lobed shape with dihedral symmetry D_q . One boundary condition is in the form (3.5). If we consider a periodic shape with q lobes and p gores per lobe where p, q are positive integers and $pq = N$, the second boundary condition implies that $\mathbf{x}(\Sigma_q)$ lies in the $y = \tan(\pi/q)x$ plane, i.e., $g_2 = \mathbf{x}(u, v) \cdot (\mathbf{j} - \tan(\pi/q)\mathbf{i}) = 0$ for $(u, v) \in \Sigma_q$. In this case, no geometric constraints are placed on tendons interior to the fundamental region.

Remark 2 Although the equilibrium state of the balloon envelope will not have self-intersections, we do not put this restriction on $\mathbf{x}(\Omega)$ for $\mathbf{x} \in \mathcal{D}$. However, we do require $\mathbf{x}(\Omega)$ for an equilibrium

state to be free of self intersections. A common theoretical and numerical approach to solving a membrane problem is to begin with an equilibrium configuration defined by a mapping, say \mathbf{y}_0 . A small increment is then added to the load and the corresponding displacement \mathbf{v}^1 is determined for the new equilibrium, $\mathbf{y}_0 + \mathbf{v}^1$. The process is continued, and at each stage, \mathbf{v}^k is computed for $k = 1, \dots, n$. The final solution is $\mathbf{y}_0 + \sum_{k=1}^n \mathbf{v}^k$. Because each intermediate solution must be an equilibrium solution, certain kinematical constraints are placed on the \mathbf{v}^k 's. In particular, each displacement field \mathbf{v}^k cannot give rise to an equilibrium state with self intersections. If a solution is desired whose load is much larger than the one corresponding to \mathbf{y}_0 , the number of intermediate steps could be large. By allowing self-intersections in the class of admissible displacements, we are able to proceed in a more direct fashion to the desired solution. This has the advantage of reducing the computation time. Although we allow intermediate configurations with self-intersections, in the end, we require that the equilibrium configuration is free of self-intersections. Note, a final solution could have regions of self-contact (see, e.g., [7]), but this could be described via local constraints in the form (3.4). In this paper, the balloons are fully deployed so the contact problem does not come into play.

3.2 Mathematical formulation

Although film and tendon weight considerations are relevant to the shape finding process, they are not significant factors in a stress analysis for the applications in this paper, and for this reason, the film and tendon weight gravitational potential energies are not included here. We define the total potential energy of a balloon configuration for a deformation mapping \mathbf{x} by $\mathcal{E}_T = \mathcal{E}_T(\mathbf{x}, \nabla \mathbf{x})$, where

$$\mathcal{E}_T = E_P + S_f, \quad (3.7)$$

E_P is the hydrostatic pressure potential due to the lifting gas and S_f is the balloon film strain energy. Next, we discuss the properties of E_P and S_f .

3.2.1 Hydrostatic pressure potential

We follow the convention for hydrostatic differential pressure P that $-P(z) > 0$ means that the inside of the balloon is pushing outward at height z units above the base of the balloon. For a super-pressure balloon, $-P(z) = bz + p_0$ where $b > 0$ is the specific buoyancy and $p_0 > 0$. Typically, $p_0 \gg bz_{top}$. In a ZPNS balloon, $p_0 = 0$. In our choice of coordinates, we assume that the base of

the balloon is fixed and corresponds to $z = 0$, so that the potential for hydrostatic pressure $P(z)$ is (see [19])

$$E_P = \int_D P(z) dV = - \int_D (bz + p_0) dV, \quad (3.8)$$

where D is the region occupied by the gas bubble. Using the divergence theorem, (3.8) can be replaced by

$$E_P = - \int_{\mathcal{S}} \left(\frac{1}{2}bz^2 + p_0z \right) \mathbf{k} \cdot \mathbf{n} dS, \quad (3.9)$$

where \mathbf{n} is the outward unit normal to \mathcal{S} , dS is surface area measure on \mathcal{S} , and $\partial D = \mathcal{S}$. The pressure distribution in an open system (i.e., without volume constraint) can be expressed as

$$P(\mathbf{x}) = -(b\mathbf{x} \cdot \mathbf{k} + p_0). \quad (3.10)$$

Note that while b and p_0 are known, the pressure potential depends on D . We can generalize the discussion by allowing a pressure distribution in the form $P(\mathbf{x}) = \operatorname{div}(\mathbf{A}(\mathbf{x}))$, but for (3.10), we see

$$\mathbf{A}(\mathbf{x}) = - \left(\frac{1}{2}b(\mathbf{x} \cdot \mathbf{k})^2 + p_0(\mathbf{x} \cdot \mathbf{k}) \right) \mathbf{k}. \quad (3.11)$$

Note, \mathbf{A} is not unique. If P is given by (3.10), then by the divergence theorem, we have

$$\begin{aligned} E_P(\mathbf{x}, \nabla \mathbf{x}) &= \int_D P(\mathbf{x}) dV \\ &= \int_{\Omega} f_P(\mathbf{x}, \nabla \mathbf{x}) dA, \end{aligned} \quad (3.12)$$

where

$$f_P(\mathbf{x}, \nabla \mathbf{x}) = g_P(\mathbf{x}, \operatorname{adj}_2 \nabla \mathbf{x}), \quad (3.13)$$

$$g_P(\mathbf{x}, \mathbf{A}) = - \left(\frac{1}{2}b(\mathbf{x} \cdot \mathbf{k})^2 + p_0(\mathbf{x} \cdot \mathbf{k}) \right) \mathbf{k} \cdot \mathbf{A}. \quad (3.14)$$

By [16, p. 117, Theorem 1.5], it follows that $f_P(\mathbf{x}, \cdot) : \mathbb{R}^{3,2} \rightarrow \mathbb{R}$ is polyaffine. However, f_P polyaffine implies f_P and $-f_P$ are polyconvex. Hence, f_P is quasiconvex [16, p. 97].

Next, we establish a few inequalities. Since

$$|\operatorname{adj}_2 \nabla \mathbf{x} \cdot \mathbf{k}| = |\mathbf{x}_{,1} \times \mathbf{x}_{,2} \cdot \mathbf{k}| \leq |\nabla \mathbf{x}|^2, \quad (3.15)$$

it follows that

$$- \left(\frac{1}{2}b|\mathbf{x}|^2 + |p_0| |\mathbf{x}| \right) |\nabla \mathbf{x}|^2 \leq g_P(\mathbf{x}, \operatorname{adj}_2 \nabla \mathbf{x}) \leq \left(\frac{1}{2}b|\mathbf{x}|^2 + |p_0| |\mathbf{x}| \right) |\nabla \mathbf{x}|^2. \quad (3.16)$$

If $|\mathbf{x}| \leq R$, then

$$- \left(\frac{1}{2}bR^2 + |p_0|R \right) |\nabla \mathbf{x}|^2 \leq g_P(\mathbf{x}, \operatorname{adj}_2 \nabla \mathbf{x}) \leq \left(\frac{1}{2}bR^2 + |p_0|R \right) |\nabla \mathbf{x}|^2. \quad (3.17)$$

Remark 3 Note, for a fully inflated shape $p_0 \geq 0$, but if the balloon is not fully inflated, it is possible for $p_0 < 0$.

3.2.2 Balloon film strain energy

Using methods in asymptotic analysis, Ciarlet derives the two-dimensional Koiter equations for a nonlinearly elastic shell in [12, Chapter 10]. The total energy of a shell of thickness 2ε for an appropriate displacement field \mathbf{u} is

$$\begin{aligned} \mathbf{u} \rightarrow & \frac{\varepsilon}{8} \int_{\Omega} E^{\alpha\beta\sigma\tau,\varepsilon} (a_{\sigma\tau}(\mathbf{u}) - a_{\sigma\tau}) (a_{\alpha\beta}(\mathbf{u}) - a_{\alpha\beta}) \sqrt{a} dy \\ & + \frac{\varepsilon^3}{6} \int_{\Omega} E^{\alpha\beta\sigma\tau,\varepsilon} (b_{\sigma\tau}(\mathbf{u}) - b_{\sigma\tau}) (b_{\alpha\beta}(\mathbf{u}) - b_{\alpha\beta}) \sqrt{a} dy, \end{aligned} \quad (3.18)$$

where λ^ε and μ^ε are the Lamé constants, and $E^{\alpha\beta\sigma\tau,\varepsilon}$ is the two-dimensional elasticity tensor of an isotropic shell,

$$E^{\alpha\beta\sigma\tau,\varepsilon} := \frac{4\lambda^\varepsilon\mu^\varepsilon}{\lambda^\varepsilon + 2\mu^\varepsilon} a^{\alpha\beta} a^{\sigma\tau} + 2\mu^\varepsilon (a^{\alpha\sigma} a^{\beta\tau} + a^{\alpha\tau} a^{\beta\sigma}). \quad (3.19)$$

When applied to the balloon problem, we can ignore the second term in (3.18), because ε^2 is extremely small, i.e., we can ignore the bending or flexural energy. In our problem formulation, the natural state is the flat reference configuration. Thus, $a_{\alpha\beta} = \delta_\beta^\alpha$ where $\delta_1^1 = \delta_2^2 = 1$ and $\delta_1^2 = \delta_2^1 = 0$. We can express the strain energy in terms of a deformation from the natural state, i.e.,

$$\mathbf{x} \rightarrow \frac{\varepsilon}{8} \int_{\Omega} E^{\alpha\beta\sigma\tau,\varepsilon} (\mathbf{x}_\sigma \cdot \mathbf{x}_\tau - \delta_\tau^\sigma) (\mathbf{x}_\alpha \cdot \mathbf{x}_\beta - \delta_\beta^\alpha) dA, \quad (3.20)$$

recognizing that $\gamma_{\alpha\beta} = \frac{1}{2} (\mathbf{x}_\alpha \cdot \mathbf{x}_\beta - \delta_\beta^\alpha)$ is the Cauchy-Green strain. Note, we do not linearize the Cauchy-Green strain in terms of the displacement field.

The Lamé constants are related to the Young's modulus E and Poisson's ratio ν , via

$$\begin{aligned} \lambda &= \frac{E\nu}{(1+\nu)(1-2\nu)}, & E &= \frac{\mu(3\lambda+2\mu)}{\lambda+\mu}, \\ \mu &= \frac{E}{2(1+\nu)}, & \nu &= \frac{\mu}{2(\lambda+\mu)}, \end{aligned} \quad (3.21)$$

where we have dropped the dependence on ε , since we assume that the physical constants have been determined for a shell of fixed thickness. Previous work on balloons (see, e.g., [5]-[9]) utilized the expression in (3.20) for the total strain energy of the balloon membrane. For the convenience of the reader, we derive an expression for (3.20) that is consistent with the formulation in [5]-[9].

We write the film strain energy S_f in the form

$$S_f = \int_{\Omega} W_f dA, \quad (3.22)$$

where

$$W_f = \frac{1}{2} \mathbf{n} : \boldsymbol{\gamma}. \quad (3.23)$$

In (3.23), \mathbf{n} represents the Second Piola-Kirchoff stress tensor, $\boldsymbol{\gamma}$ represents the Cauchy-Green strain tensor, and ‘:’ is the tensor inner product. The contravariant components of \mathbf{n} are denoted by $n^{\alpha\beta}$, the covariant components of $\boldsymbol{\gamma}$ are denoted by $\gamma_{\alpha\beta}$, and $\mathbf{n} : \boldsymbol{\gamma} = n^{\alpha}_{\beta} \gamma^{\beta}_{\alpha}$. Assuming a linear elastic isotropic material, we have

$$n^{\alpha\beta} = E^{\alpha\beta\lambda\mu} \gamma_{\lambda\mu}, \quad (3.24)$$

where $E^{\alpha\beta\lambda\mu}$ is the tensor of elastic moduli, i.e.,

$$E^{\alpha\beta\lambda\mu} = \frac{tE}{2(1+\nu)} \left[a^{\alpha\lambda} a^{\beta\mu} + a^{\alpha\mu} a^{\beta\lambda} + \frac{2\nu}{1-\nu} a^{\alpha\beta} a^{\lambda\mu} \right], \quad (3.25)$$

$t = 2\varepsilon$ is the shell thickness, and $a_{\alpha\beta} = \delta_{\beta}^{\alpha}$. Setting $2\varepsilon = t$ and using the relations (3.21), we find that (3.19) and (3.25) are equivalent. In matrix form, the right Cauchy-Green deformation tensor is

$$\mathbf{C} = \mathbf{F}^T \mathbf{F},$$

where $\nabla \mathbf{x} = \mathbf{F}$ is the deformation gradient and the Cauchy-Green strain ($\boldsymbol{\gamma}$) is

$$\mathbf{G} = \frac{1}{2} (\mathbf{C} - \mathbf{I}).$$

Assuming an isotropic film and the linear stress-strain relation in (3.24), the Second Piola-Kirchoff stress can be written in matrix form as

$$\mathbf{S} = \tau \left[\mathbf{G} + \nu \text{Cof}(\mathbf{G})^T \right], \quad (3.26)$$

where

$$\tau = \frac{tE}{1-\nu^2}, \quad (3.27)$$

and the 2×2 cofactor matrix is

$$\text{Cof} \left(\begin{bmatrix} a_{11} & a_{12} \\ a_{21} & a_{22} \end{bmatrix} \right) = \begin{bmatrix} a_{22} & -a_{12} \\ -a_{21} & a_{11} \end{bmatrix}.$$

\mathbf{G} and \mathbf{S} are symmetric and by the spectral representation theorem, we have

$$\begin{aligned} \mathbf{G} &= \delta_1 \mathbf{n}_1 \otimes \mathbf{n}_1 + \delta_2 \mathbf{n}_2 \otimes \mathbf{n}_2, \\ \mathbf{S} &= \mu_1 \mathbf{n}_1 \otimes \mathbf{n}_1 + \mu_2 \mathbf{n}_2 \otimes \mathbf{n}_2, \end{aligned}$$

where \mathbf{n}_1 and \mathbf{n}_2 are orthonormal vectors. The eigenvalues of \mathbf{S} (denoted by $\mu_1 = \tau(\delta_1 + \nu\delta_2)$ and $\mu_2 = \tau(\delta_2 + \nu\delta_1)$) are the principal stress resultants and the eigenvalues of \mathbf{G} (denoted by δ_1 and

δ_2) are principal strains. Because we have assumed a linear stress-strain constitutive relation and an isotropic film, \mathbf{S} and \mathbf{G} have the same principle axes. The eigenvalues of \mathbf{C} are the Cauchy strains which are denoted by λ_i^2 where $\delta_i = \frac{1}{2}(\lambda_i^2 - 1)$ and $\delta_i \geq -\frac{1}{2}$. The film strain density is given by

$$W_f = \frac{1}{2}\mathbf{S} : \mathbf{G}. \quad (3.28)$$

In terms of the Cauchy-Green strains δ_i , the standard membrane strain energy is given by

$$W_f(\delta_1, \delta_2) = \frac{tE}{2(1-\nu^2)} \left(\delta_1^2 + \delta_2^2 + 2\nu\delta_1\delta_2 \right), \quad (3.29)$$

while in terms of the Cauchy strains, we have

$$W_f(\lambda_1, \lambda_2) = \frac{1}{8}\tau \left(\lambda_1^4 + \lambda_2^4 + 2\nu\lambda_1^2\lambda_2^2 - 2(1+\nu) \left(\lambda_1^2 + \lambda_2^2 \right) + 2(1+\nu) \right). \quad (3.30)$$

Next, we derive a few estimates that will be needed at a later time. From the definition of $|\mathbf{F}|$, we have

$$|\mathbf{F}|^2 = \lambda_1^2 + \lambda_2^2.$$

It follows that for $0 < \nu < 1$

$$\lambda_1^4 + \lambda_2^4 + 2\lambda_1^2\lambda_2^2 > \lambda_1^4 + \lambda_2^4 + 2\nu\lambda_1^2\lambda_2^2 > \nu(\lambda_1^4 + \lambda_2^4) + 2\nu\lambda_1^2\lambda_2^2 = \nu|\mathbf{F}|^4. \quad (3.31)$$

From (3.30) and (3.31), we can find a lower bound for W_f , i.e.,

$$W_f \geq \frac{1}{8}\tau \left(\nu|\mathbf{F}|^4 - 2(1+\nu)|\mathbf{F}|^2 + 2(1+\nu) \right). \quad (3.32)$$

Applying (3.31) and (3.32), we are led to

$$\frac{1}{8}\tau \left(\nu|\mathbf{F}|^4 - 2(1+\nu)|\mathbf{F}|^2 + 2(1+\nu) \right) \leq W_f \leq \frac{1}{8}\tau|\mathbf{F}|^4 + \frac{1}{4}\tau(1+\nu). \quad (3.33)$$

We conclude this subsection with a lemma that will be useful in obtaining our existence results.

Lemma 2 *Let $\kappa_1, \kappa_2 > 0$.*

(i) *There exist α, ρ, γ such that*

$$\alpha|u|^4 - \rho \leq \kappa_1|u|^4 - \kappa_2|u|^2 \leq \gamma|u|^4, \quad (3.34)$$

$$0 < \alpha < \kappa_1 < \gamma, \text{ and } \rho = \kappa_2^2/4(\kappa_1 - \alpha).$$

(ii) *There exist constants γ, ρ such that*

$$\kappa_1|u|^4 + \kappa_2|u|^2 \leq \gamma|u|^4 + \rho, \quad (3.35)$$

$$0 < \kappa_1 < \gamma \text{ and } \rho = \kappa_2^2/4(\gamma - \kappa_1).$$

Part (i). The second inequality in (3.34) is obvious. If $-\rho = \inf_u\{(\kappa_1 - \alpha)|u|^4 - \kappa_2|u|^2\} > -\infty$, then we are done. Otherwise, it's easy to show that $g(x) = (\kappa_1 - \alpha)x^4 - \kappa_2x^2$ has an absolute minimum at $x_0 = \sqrt{\kappa_2/2(\kappa_1 - \alpha)}$ and $g(x_0) = -\kappa_2^2/4(\kappa_1 - \alpha)$. The first inequality in (3.34) follows with $-\rho = g(x_0)$. The proof of Part (ii) follows the proof of Part (i).

3.2.3 Relaxation of the film strain energy density

The energy density in (3.28) can lead to states where μ_1 or μ_2 are negative, corresponding to a compression. While this is reasonable for certain types of shells, the balloon film cannot support such a compression. Instead, the film will form folds or wrinkle. To tackle the problem of negative compressive stresses, we follow the methods introduced by A. C. Pipkin (see [24]). In the following, let δ_1 and δ_2 be the principal (Cauchy-Green) strains for a typical facet T in a triangulation of Ω . Let μ_1 and μ_2 be the corresponding principal stress resultants. In Pipkin's approach, a membrane M is decomposed into three distinct regions:

S - slack region ($\delta_1 < 0, \delta_2 < 0$),

T - tense region ($\mu_1 > 0, \mu_2 > 0$), and

U - wrinkled region ($U = M \setminus S \cup T$).

We apply this classification scheme to each T in our triangulation of Ω . On S the strain energy is assumed to be zero and on T the relaxed strain energy density is exactly the same as the standard strain energy density. On the region U, a modified Cauchy-Green strain \mathbf{G}^* is introduced. If \mathbf{G} is the usual Cauchy-Green strain, then

$$\mathbf{G}^* = \mathbf{G} + \beta^2 \mathbf{n} \otimes \mathbf{n},$$

where \mathbf{n} and \mathbf{t} are (unknown) principal stress directions based on \mathbf{G}^* . Pipkin refers to $-\beta^2 \mathbf{n} \otimes \mathbf{n}$ as the wrinkling strain and \mathbf{G}^* as the elastic strain. The elastic strain is thought to represent the straining in an "averaged" wrinkled surface and leads to uniaxial stress on U in the form:

$$\mathbf{S}^* = \mu \mathbf{t} \otimes \mathbf{t},$$

where $\mu > 0$ and \mathbf{t} is a unit vector orthogonal to \mathbf{n} . For our exposition, we assume that \mathbf{t} is the tensile direction, and \mathbf{n} is a unit vector orthogonal to \mathbf{t} . The parameter β^2 and \mathbf{n} are chosen in such a way that the following conditions are satisfied.

$$\begin{aligned}\mathbf{n} \cdot \mathbf{S}^* \mathbf{n} &= 0, \\ \mathbf{n} \cdot \mathbf{S}^* \mathbf{t} &= 0.\end{aligned}$$

For an isotropic material, \mathbf{S}^* can be written in the form:

$$\mathbf{S}^* = \mathbf{S} + \tau\beta^2 \left(\mathbf{n} \otimes \mathbf{n} + \nu \text{Cof}(\mathbf{n} \otimes \mathbf{n})^T \right),$$

and it follows that

$$\beta^2 = -\frac{1}{\tau} \mathbf{n} \cdot \mathbf{S} \mathbf{n}. \quad (3.36)$$

If $W_f = W_f(\mathbf{G})$, its relaxation is $W_f^* = W_f(\mathbf{G}^*)$ where \mathbf{G}^* uses β^2 from (3.36) and \mathbf{t} is the principal direction that corresponds to a positive principal strain. One can show that on \mathbf{U} , the principal strains of \mathbf{G}^* are in the form $\{\delta_2, -\nu\delta_2\}$ or $\{\delta_1, -\nu\delta_1\}$ (see [15]). The principal stresses of $\mathbf{S}^* = \mathbf{S}(\mathbf{G}^*)$ are given by

$$\mathbf{S}^* = \begin{cases} 0, & \delta_1 < 0 \text{ and } \delta_2 < 0, \\ tE\delta_2 \mathbf{n}_2 \otimes \mathbf{n}_2, & \mu_1 \leq 0 \text{ and } \delta_2 \geq 0, \\ tE\delta_1 \mathbf{n}_1 \otimes \mathbf{n}_1, & \mu_2 \leq 0 \text{ and } \delta_1 \geq 0, \\ \mu_1 \mathbf{n}_1 \otimes \mathbf{n}_1 + \mu_2 \mathbf{n}_2 \otimes \mathbf{n}_2, & \mu_1 \geq 0 \text{ and } \mu_2 \geq 0. \end{cases} \quad (3.37)$$

Wrinkling is modeled by replacing W_f with W_f^* where

$$W_f^*(\delta_1, \delta_2; t, \nu, E) = \begin{cases} 0, & \delta_1 < 0 \text{ and } \delta_2 < 0, \\ \frac{1}{2}tE\delta_2^2, & \mu_1 \leq 0 \text{ and } \delta_2 \geq 0, \\ \frac{1}{2}tE\delta_1^2, & \mu_2 \leq 0 \text{ and } \delta_1 \geq 0, \\ \frac{tE}{2(1-\nu^2)}(\delta_1^2 + \delta_2^2 + 2\nu\delta_1\delta_2), & \mu_1 \geq 0 \text{ and } \mu_2 \geq 0. \end{cases} \quad (3.38)$$

In order to obtain existence results, we will need upper and lower bounds on W_f^* in terms of $|\nabla \mathbf{x}|$. Since W_f^* is the largest convex function not exceeding W_f , we have

$$W_f^* \leq W_f. \quad (3.39)$$

To obtain a lower bound for W_f^* , we consider the following. Let

$$\begin{aligned}\Lambda &= \{(\delta_1, \delta_2) \mid \delta_1 \geq -\frac{1}{2}, \delta_2 \geq -\frac{1}{2}\} \\ \Lambda_1 &= \{(\delta_1, \delta_2) \in \Lambda \mid \delta_2 > -\delta_1/\nu, \delta_2 > -\nu\delta_1\}, \\ \Lambda_2 &= \Lambda \setminus \Lambda_1.\end{aligned}$$

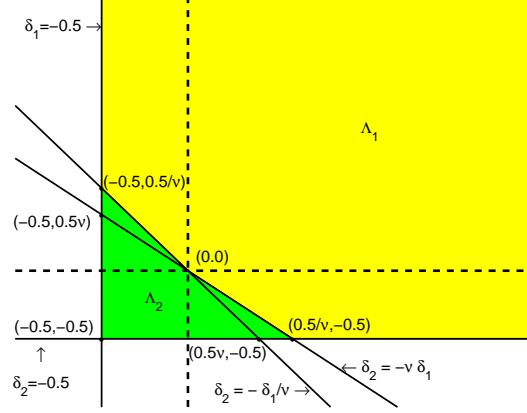


Figure 5: (δ_1, δ_2) - domain for W_f and W_f^*

See Figure 5. While Λ_1 is unbounded, $W_f = W_f^*$ for $(\delta_1, \delta_2) \in \Lambda_1$. Since Λ_2 is compact, there is a constant d such that

$$d = \max_{(\delta_1, \delta_2) \in \Lambda_2} \{W_f(\delta_1, \delta_2) - W_f^*(\delta_1, \delta_2)\}.$$

$W_f(\delta_1, \delta_2)$ has a critical point when $\delta_1 + \nu\delta_2 = 0$ and $\delta_2 + \nu\delta_1 = 0$. Thus, $(\delta_1, \delta_2) = (0, 0)$ is the only critical point. Hence, d is achieved on the boundary of Λ_2 at a corner point. By inspection, one finds d is achieved at $(-0.5, -0.5)$, $W_f^*(-0.5, -0.5) = 0$, and $d = \frac{1}{4}\tau(1 + \nu)$. Thus,

$$W_f \leq W_f^* + \frac{1}{4}\tau(1 + \nu), \quad (\delta_1, \delta_2) \in \Lambda. \quad (3.40)$$

Combining (3.39)-(3.40), yields

$$W_f - \frac{1}{4}\tau(1 + \nu) \leq W_f^* \leq W_f. \quad (3.41)$$

We conclude this subsection by noting if f is quasi-convex, so is $f + C$ for any $C \in \mathbb{R}$, for if

$$\int_D f(u_0, v_0, \mathbf{x}_0, \boldsymbol{\xi}_0 + \nabla \mathbf{x}(y)) dy \geq |D|f(u_0, v_0, \mathbf{x}_0),$$

for every cube $D \subset \Omega$, for every $(u_0, v_0, \mathbf{x}_0, \boldsymbol{\xi}_0) \in \Omega \times \mathbb{R}^m \times \mathbb{R}^{nm}$ and for every $\mathbf{x} \in W_0^{1,\infty}(D; \mathbb{R}^m)$, then

$$\int_D (f(u_0, v_0, \mathbf{x}_0, \boldsymbol{\xi}_0 + \nabla \mathbf{x}(y)) + C) dy \geq |D|(f(u_0, v_0, \mathbf{x}_0) + C).$$

3.3 Constraints

3.3.1 Tendon constraint

Tendons are included in our balloon model through the use of constraints. We assume that a tendon is encased in a sleeve that is attached along the seam between two adjacent gores. We assume that

the tendons are connected to a common point at the top of the balloon and to a bottom end-plate. The top of the balloon is free to move up and down the z axis and the bottom end-plate is fixed at the level $z = 0$.

Remark 4 The interaction between the tendon and film is very complicated. Even without tacking to the sleeve, a tendon will not slide freely within its sleeve when a pumpkin balloon is fully inflated. The same can be said for a zero-pressure balloon which uses a load tape, a one-dimensional structural element that serves the same function as a load tendon. For simplicity, we have used the same tendon model for both the ZPNS and the pumpkin balloon. The assumption of constant tension enables us to include stiff tendons in the present model and analyze equilibrium configurations of a strained fully inflated shape.

We first consider a single tendon in the deformed state $\mathbf{x}(\Sigma_i)$ for $\mathbf{x} \in \mathcal{D}$. By the Sobolev Embedding Theorem (see, e.g., [20, Theorem 7.26, p. 171]; for a manifold setting, see [3, Theorem 2.34, p. 55]), $W^{1,4}(\Omega)$ is compactly embedded in $C^{0,\beta}(\bar{\Omega})$ for any $0 < \beta < 1/2$. Hence, $\mathbf{x} \in X$ (or $X_{\mathbf{g}}$) implies that $\mathbf{x} \in C^{0,\beta}(\bar{\Omega}, \mathbb{R}^3)$, and in particular, $\boldsymbol{\alpha}_i(v) = \mathbf{x}|_{\Sigma_i}$ is well-defined and Hölder continuous. The length of $\mathbf{x}(\Sigma_i)$ is denoted by $L[\Sigma_i]$. A tendon is under constant tension, and the strain in the i th tendon is

$$\epsilon_i = (L[\Sigma_i] - L_t) / L_t. \quad (3.42)$$

In our numerical model, $L[\Sigma_i]$ is approximated by

$$L[\Sigma_i] \approx \sum_{j=1}^n |\boldsymbol{\alpha}_i(v_j) - \boldsymbol{\alpha}_i(v_{j-1})|$$

where $\{v_j\}$ is a partition of $[0, L_c]$, i.e., $0 = v_0 < v_1 < \dots < v_{n-1} < v_n = L_c$.

The strain energy in a tendon of length L_t with stiffness K is $S_{t,i} = S_t[\Sigma_i] = \frac{1}{2}K\epsilon_i^2L_t$. K has the units of force. Since the tendon cannot support compression, we utilize the relaxed tendon strain energy

$$S_{t,i}^* = \begin{cases} \frac{1}{2}K\epsilon_i^2L_t, & \epsilon_i > 0, \\ 0, & \epsilon_i \leq 0. \end{cases} \quad (3.43)$$

Since we assume that the tendons are inextensible, we set $K = 1$ and impose the conditions

$$S_{t,i}^* \leq 0, \quad i = 1, 2, \dots, N, \quad (3.44)$$

which can be included as local constraints in the form of (3.4). Because we are not using $\nabla \mathbf{x}$ to calculate the arc length of tendons, a continuity argument similar to the one used in Section 3

shows $X_{\mathbf{g}}$ is closed when $\mathbf{g} \leq \mathbf{0}$ includes a constraint in the form (3.44). Consider (3.7) subject to constraints in the form of (3.44). Let \mathbf{x} be a minimizer of this system where $\lambda_i, i = 1, \dots, N$ are the corresponding Lagrange multipliers. We can interpret the λ_i 's in

$$E_T(\mathbf{x}, \nabla \mathbf{x}) + \sum_{i=1}^N \lambda_i S_{t,i}^* \quad (3.45)$$

as the tendon stiffnesses that are needed to maintain equilibrium. In our numerical simulations presented here, we will consider cyclically symmetric solutions so only one tendon constraint is needed. Note, tendons are modeled in a different fashion in [6]-[9], but our results here are consistent with those works when a very large value of K is used. We carried out numerical simulations when (3.44) is replaced by an equality constraint and obtained essentially the same results as the ' \leq ' case with $\epsilon_1 \approx 10^{-10}$ m/m. If we drop the requirement that the tendons are inextensible, we can replace the ' \leq ' in (3.44) with ' \geq '. In this case, we find $S_{t,i}^* > 0$ for the solution where $\epsilon_1 \approx 0.005$ m/m.

3.3.2 Volume constraint

In an open system such as the ZPNS design, the balloon is open to the atmosphere at $z = 0$. This means that the volume of the balloon at equilibrium will adjust itself accordingly. In a closed system, the volume is fixed, and p_0 is determined. Using the divergence theorem, the volume of the balloon \mathcal{S} can be expressed as

$$V(\mathbf{x}) = \int_D 1 \, dV = \frac{1}{3} \int_S \mathbf{x} \cdot \mathbf{n} \, dS = \int_{\Omega} f_V(\mathbf{x}, \nabla \mathbf{x}) \, dA \quad (3.46)$$

where $\mathbf{n} \, dS = \text{adj}_2 \nabla \mathbf{x} \, dA$ and $f_V(\mathbf{x}, \nabla \mathbf{x}) = g_V(\mathbf{x}, \text{adj}_2 \nabla \mathbf{x})$,

$$g_V(\mathbf{x}, \mathbf{A}) = \frac{1}{3} \mathbf{x} \cdot \mathbf{A}. \quad (3.47)$$

The same argument used to show f_P is quasiconvex, shows $f_V(\mathbf{x}, \cdot)$ is quasiconvex. (3.46) can be evaluated exactly when \mathcal{S} is a faceted surface. The volume constraint is in the form,

$$V(\mathbf{x}) - \omega_0 = 0, \quad (3.48)$$

where ω_0 is the target volume.

In a closed system where (3.48) holds and p_0 is unknown, we can assume $-P(z) = bz$. After finding an equilibrium solution by minimizing (3.7) subject to (3.48), we find that the Lagrange multiplier λ in

$$\mathcal{E}_T(\mathbf{x}, \nabla \mathbf{x}) + \lambda(V(\mathbf{x}) - \omega_0)$$

yields the appropriate constant pressure term that is needed for equilibrium. Although we use Lagrange multipliers to handle constraints in our numerical approach, our theoretical model incorporates such a constraint directly into the underlying solution space.

Before we demonstrate that the volume constraint can be included in the definition of $X_{\mathbf{g}}$, we will need an estimate for $|\text{adj}_2 \mathbf{A} - \text{adj}_2 \mathbf{B}|$.

Lemma 3 *Let $\mathbf{A}, \mathbf{B} \in \mathbb{R}^{nm}$. There exists a constant $\tilde{\beta} > 0$ independent of \mathbf{A}, \mathbf{B} such that*

$$|\text{adj}_2 \mathbf{A} - \text{adj}_2 \mathbf{B}| \leq \tilde{\beta}(|\mathbf{A}| + |\mathbf{B}|)|\mathbf{A} - \mathbf{B}|. \quad (3.49)$$

When $nm = 6$, $\tilde{\beta} = 3$.

We establish the proof for the case $nm = 6$, but it is straightforward to modify the argument for general nm . For $\begin{pmatrix} x_1 & x_2 \\ x_3 & x_4 \\ x_5 & x_6 \end{pmatrix} \in \mathbb{R}^{3,2}$, consider $\mathbf{X} = [x_1, x_2, \dots, x_6]^T$. Define $\mathbf{f}(\mathbf{X}) = [f_1(\mathbf{X}), f_2(\mathbf{X}), f_3(\mathbf{X})]^T = \text{adj}_2 \mathbf{X}$ where $f_1(\mathbf{X}) = x_3x_6 - x_4x_5$, $f_2(\mathbf{X}) = -(x_1x_6 - x_2x_5)$, $f_3(\mathbf{X}) = x_1x_4 - x_2x_3$. For f_1 , we see $Df_1(\mathbf{X}) = [0, 0, x_6, -x_5, -x_4, x_3]^T$. Since $D^2f_1(\mathbf{X})$ is independent of \mathbf{X} , we write $D^2f_1(\mathbf{X}) = \mathbf{H}_1$, where

$$\mathbf{H}_1 = \begin{pmatrix} 0 & 0 & 0 & 0 & 0 & 0 \\ 0 & 0 & 0 & 0 & 0 & 0 \\ 0 & 0 & 0 & 0 & 0 & 1 \\ 0 & 0 & 0 & 0 & -1 & 0 \\ 0 & 0 & 0 & -1 & 0 & 0 \\ 0 & 0 & 1 & 0 & 0 & 0 \end{pmatrix}.$$

One easily obtains $f_1(\mathbf{X}) = \frac{1}{2}\mathbf{X}^T \mathbf{H}_1 \mathbf{X}$. For $i = 2, 3$, we find $D^2f_i(\mathbf{X}) = \mathbf{H}_i$ and $f_i(\mathbf{X}) = \frac{1}{2}\mathbf{X}^T \mathbf{H}_i \mathbf{X}$, where

$$\mathbf{H}_2 = \begin{pmatrix} 0 & 0 & 0 & 0 & 0 & -1 \\ 0 & 0 & 0 & 0 & 1 & 0 \\ 0 & 0 & 0 & 0 & 0 & 0 \\ 0 & 0 & 0 & 0 & 0 & 0 \\ 0 & 1 & 0 & 0 & 0 & 0 \\ -1 & 0 & 0 & 0 & 0 & 0 \end{pmatrix} \quad \text{and} \quad \mathbf{H}_3 = \begin{pmatrix} 0 & 0 & 0 & 1 & 0 & 0 \\ 0 & 0 & -1 & 0 & 0 & 0 \\ 0 & -1 & 0 & 0 & 0 & 0 \\ 1 & 0 & 0 & 0 & 0 & 0 \\ 0 & 0 & 0 & 0 & 0 & 0 \\ 0 & 0 & 0 & 0 & 0 & 0 \end{pmatrix}.$$

Using the properties of $\mathbf{f}(\mathbf{A})$ and $\mathbf{f}(\mathbf{B})$, we obtain

$$\begin{aligned} |\mathbf{f}(\mathbf{A}) - \mathbf{f}(\mathbf{B})| &= |(f_1(\mathbf{A}) - f_1(\mathbf{B}), f_2(\mathbf{A}) - f_2(\mathbf{B}), f_3(\mathbf{A}) - f_3(\mathbf{B}))| \\ &= \frac{1}{2} \left| \left(\mathbf{A}^T \mathbf{H}_1 (\mathbf{A} - \mathbf{B}) + (\mathbf{A} - \mathbf{B})^T \mathbf{H}_1 \mathbf{B}, \right. \right. \\ &\quad \left. \mathbf{A}^T \mathbf{H}_2 (\mathbf{A} - \mathbf{B}) + (\mathbf{A} - \mathbf{B})^T \mathbf{H}_2 \mathbf{B}, \right. \\ &\quad \left. \mathbf{A}^T \mathbf{H}_3 (\mathbf{A} - \mathbf{B}) + (\mathbf{A} - \mathbf{B})^T \mathbf{H}_3 \mathbf{B} \right) \end{aligned}$$

$$\begin{aligned}
&\leq \frac{1}{2} \left(\sum_{i=1}^3 |\mathbf{A}^T \mathbf{H}_i (\mathbf{A} - \mathbf{B}) + (\mathbf{A} - \mathbf{B})^T \mathbf{H}_i \mathbf{B}|^2 \right)^{1/2} \\
&\leq \frac{1}{2} \left(\sum_{i=1}^3 |\mathbf{A}^T \mathbf{H}_i (\mathbf{A} - \mathbf{B}) + (\mathbf{A} - \mathbf{B})^T \mathbf{H}_i \mathbf{B}| \right) \\
&= \frac{1}{2} \sum_{i=1}^3 |\mathbf{H}_i| (|\mathbf{A}| + |\mathbf{B}|) |\mathbf{A} - \mathbf{B}| \\
&\leq \tilde{\beta} (|\mathbf{A}| + |\mathbf{B}|) |\mathbf{A} - \mathbf{B}|.
\end{aligned}$$

Since $|\mathbf{H}_i| = \sqrt{4} = 2$, the proof is completed with $\tilde{\beta} = 3$.

Lemma 4 *Let $V(\mathbf{x})$ be defined as in (3.46). Let $\|\mathbf{x}_k - \mathbf{x}\|_{1,4} \rightarrow 0$ where $\mathbf{x}, \mathbf{x}_k \in X$ and $V(\mathbf{x}_k) = \omega_0$, then*

$$\lim_{k \rightarrow \infty} V(\mathbf{x}_k) = V(\lim_{k \rightarrow \infty} \mathbf{x}_k) = V(\mathbf{x}) = \omega_0.$$

For each k , we have

$$\begin{aligned}
|V(\mathbf{x}) - \omega_0| &= |V(\mathbf{x}) - V(\mathbf{x}_k)| \\
&= \left| \frac{1}{3} \int_{\Omega} (\mathbf{x} \cdot \text{adj}_2 \nabla \mathbf{x} - \mathbf{x}_k \cdot \text{adj}_2 \nabla \mathbf{x}_k) dA \right|.
\end{aligned}$$

Adding and subtracting $\mathbf{x} \cdot \text{adj}_2 \nabla \mathbf{x}_k$ to this last expression and applying Lemma 3, we are led to

$$\begin{aligned}
|V(\mathbf{x}) - \omega_0| &= \left| \frac{1}{3} \int_{\Omega} (\mathbf{x} - \mathbf{x}_k) \cdot \text{adj}_2 \nabla \mathbf{x}_k + \mathbf{x} \cdot (\text{adj}_2 \nabla \mathbf{x} - \text{adj}_2 \nabla \mathbf{x}_k) dA \right| \\
&\leq \int_{\Omega} |\mathbf{x} - \mathbf{x}_k| |\nabla \mathbf{x}_k|^2 dA + \\
&\quad \int_{\Omega} |\mathbf{x}| (|\nabla \mathbf{x}| + |\nabla \mathbf{x}_k|) |\nabla \mathbf{x} - \nabla \mathbf{x}_k| dA. \tag{3.50}
\end{aligned}$$

Since $\mathbf{x}, \mathbf{x} - \mathbf{x}_k, \nabla \mathbf{x} - \nabla \mathbf{x}_k \in L^4(\Omega, \mathbb{R}^3)$, $\nabla \mathbf{x}, \nabla \mathbf{x}_k \in L^2(\Omega, \mathbb{R}^3)$, and $|\nabla \mathbf{x}_k|^2 \in L^{4/3}(\Omega, \mathbb{R}^3)$, we can apply the generalized Hölder inequality to (3.50) and obtain

$$\begin{aligned}
|V(\mathbf{x}) - \omega_0| &\leq \left(\int_{\Omega} |\mathbf{x} - \mathbf{x}_k|^4 dA \right)^{1/4} \left(\int_{\Omega} |\nabla \mathbf{x}_k|^{\frac{8}{3}} dA \right)^{3/4} + \\
&\quad \left(\int_{\Omega} |\mathbf{x}|^4 dA \right)^{1/4} \left[\left(\int_{\Omega} |\nabla \mathbf{x}|^2 dA \right)^{1/2} + \right. \\
&\quad \left. \left(\int_{\Omega} |\nabla \mathbf{x}_k|^2 dA \right)^{1/2} \right] \left(\int_{\Omega} |\nabla \mathbf{x} - \nabla \mathbf{x}_k|^4 dA \right)^{1/4} \tag{3.51}
\end{aligned}$$

Since $\mathbf{x}_k \rightarrow \mathbf{x} \in W^{1,4}(\Omega, \mathbb{R}^3)$ and $\|\nabla \mathbf{x}_k\|_{L^4}$ is uniformly bounded, from (3.51) we see that $|V(\mathbf{x}) - \omega_0| = 0$ and the proof is complete.

Remark 5 From Lemma 4, we see that $V(\mathbf{x}) - \omega_0 = 0$ is a global constraint satisfying (3.3) in Lemma 1. When $V(\mathbf{x}) - \omega_0 = 0$ is included among the constraints, $\mathbf{g} \leq \mathbf{0}$, we denote the corresponding closed subspace of X by $X_{\mathbf{g}(\omega_0)}$ in order to emphasize the dependence on ω_0 .

4 Existence Results

In the following, we write $\mathbf{u} = (u, v) \in \Omega$. The total energy of the balloon system is taken to be the sum of the hydrostatic pressure potential and the film strain energy,

$$\mathcal{E}_T^*(\bar{\mathbf{x}}, \nabla \mathbf{x}) = \int_{\Omega} \left(W_f^*(\mathbf{u}, \mathbf{x}, \nabla \mathbf{x}) + f_P(\mathbf{x}, \nabla \mathbf{x}) \right) dA. \quad (4.1)$$

Combining (3.17) and (3.41), we find

$$W_f - \frac{1}{4}\tau(1 + \nu) - \left(\frac{1}{2}bR^2 + |p_0|R \right) |\mathbf{F}|^2 \leq W_f^* + f_P \leq W_f + \left(\frac{1}{2}bR^2 + |p_0|R \right) |\mathbf{F}|^2. \quad (4.2)$$

Next, applying the appropriate upper and lower bounds on W_f established in (3.33), we have

$$\begin{aligned} & \frac{1}{8}\tau(\nu|\mathbf{F}|^4 - 2(1 + \nu)|\mathbf{F}|^2 + 2(1 + \nu)) - \frac{1}{4}\tau(1 + \nu) - \left(\frac{1}{2}bR^2 + |p_0|R \right) |\mathbf{F}|^2 \\ & \leq W_f^* + f_P \leq \frac{1}{8}\tau|\mathbf{F}|^4 + \frac{1}{4}\tau(1 + \nu) + \left(\frac{1}{2}bR^2 + |p_0|R \right) |\mathbf{F}|^2. \end{aligned}$$

Simplifying, we have

$$\begin{aligned} & \frac{1}{8}\tau\nu|\mathbf{F}|^4 - \frac{1}{4}(\tau(1 + \nu) + 2bR^2 + 4|p_0|R) |\mathbf{F}|^2 \\ & \leq W_f^* + f_P \\ & \leq \frac{1}{8}\tau|\mathbf{F}|^4 + \frac{1}{4}\tau(1 + \nu) + \left(\frac{1}{2}bR^2 + |p_0|R \right) |\mathbf{F}|^2. \end{aligned} \quad (4.3)$$

Let $\kappa_1 = \frac{1}{8}\tau\nu$ and $\kappa_2 = \frac{1}{4}(\tau(1 + \nu) + 2bR^2 + 4|p_0|R)$ and apply Lemma 2(i) to the first inequality in (4.3). Choose α_1 so that $0 < \alpha_1 < \frac{1}{8}\tau\nu$ and define ν_1 by the relation $\alpha_1 = \frac{1}{8}\tau\nu_1$. We see that $0 < \nu_1 < \nu$ and by Lemma 2(i), we have

$$\frac{1}{8}\tau\nu_1|\mathbf{F}|^4 - \rho_1 \leq \frac{1}{8}\tau\nu|\mathbf{F}|^4 - \frac{1}{4}(\tau(1 + \nu) + 2bR^2 + 4|p_0|R) |\mathbf{F}|^2,$$

where

$$\rho_1 = \frac{(\tau(1 + \nu) + 2bR^2 + 4|p_0|R)^2}{8\tau(\nu - \nu_1)}.$$

Turning to the second inequality in (4.3), and applying Part (ii) of Lemma 2, we choose $\theta_1 > 1$, and it follows that

$$\frac{1}{8}\tau|\mathbf{F}|^4 + \left(\frac{1}{2}bR^2 + |p_0|R \right) |\mathbf{F}|^2 \leq \frac{1}{8}\tau\theta_1|\mathbf{F}|^4 + \rho_2,$$

where

$$\rho_2 = \frac{(bR^2 + 2|p_0|R)^2}{2\tau(\theta_1 - 1)}.$$

Thus,

$$\frac{1}{8}\tau\nu_1|\mathbf{F}|^4 - \rho_1 \leq W_f^* + f_P \leq \frac{1}{8}\tau\theta_1|\mathbf{F}|^4 + \rho_2 + \frac{1}{4}\tau(1 + \nu),$$

and

$$\frac{1}{8}\tau\nu_1|\mathbf{F}|^4 \leq W_f^* + f_P + \rho_1 \leq \frac{1}{8}\tau\theta_1|\mathbf{F}|^4 + \frac{1}{4}\tau(1 + \nu) + \rho_1 + \rho_2. \quad (4.4)$$

It follows that

$$f_T^*(\mathbf{u}, \mathbf{x}, \nabla \mathbf{x}) = W_f^*(\mathbf{u}, \mathbf{x}, \nabla \mathbf{x}) + f_P(\mathbf{u}, \mathbf{x}, \nabla \mathbf{x}) + \rho_1 \quad (4.5)$$

is quasiconvex and satisfies some additional properties that we summarize in the following lemma.

Lemma 5 *If $f_T^*(\mathbf{u}, \mathbf{x}, \nabla \mathbf{x}) = W_f^*(\mathbf{u}, \mathbf{x}, \nabla \mathbf{x}) + f_P(\mathbf{u}, \mathbf{x}, \nabla \mathbf{x}) + \rho_1$ and $|\mathbf{x}| < R$, then f_T^* is quasiconvex and*

$$(i) \quad \gamma|\mathbf{A}|^4 \leq f_T^*(\mathbf{u}, \mathbf{x}, \mathbf{A}) \leq \delta(1 + |\mathbf{A}|^4)$$

$$(ii) \quad |f_T^*(\mathbf{u}, \mathbf{x}, \mathbf{A}) - f_T^*(\mathbf{u}, \mathbf{y}, \mathbf{B})| \leq \beta (1 + |\mathbf{x}|^3 + |\mathbf{y}|^3 + |\mathbf{A}|^3 + |\mathbf{B}|^3) (|\mathbf{x} - \mathbf{y}| + |\mathbf{A} - \mathbf{B}|).$$

Property (i) is (4.4) with $\delta = \max\{\frac{1}{8}\tau\theta_1, \frac{1}{4}\tau(1 + \nu) + \rho_1 + \rho_2\}$ and $\gamma = \frac{1}{8}\tau\nu_1$. We will show Property (ii) as follows. Consider

$$\begin{aligned} f_T^*(\mathbf{u}, \mathbf{x}, \mathbf{A}) - f_T^*(\mathbf{u}, \mathbf{y}, \mathbf{B}) &= (W_f^*(\mathbf{u}, \mathbf{x}, \mathbf{A}) - W_f^*(\mathbf{u}, \mathbf{y}, \mathbf{B})) \\ &\quad + (f_P(\mathbf{u}, \mathbf{x}, \mathbf{A}) - f_P(\mathbf{u}, \mathbf{y}, \mathbf{B})). \end{aligned} \quad (4.6)$$

Since Lemma A.1 applies to W_f^* , there exists $\beta_1 > 0$ such that

$$|W_f^*(\mathbf{u}, \mathbf{x}, \mathbf{A}) - W_f^*(\mathbf{u}, \mathbf{y}, \mathbf{B})| \leq \beta_1(1 + |\mathbf{A}|^3 + |\mathbf{B}|^3)|\mathbf{A} - \mathbf{B}|. \quad (4.7)$$

To complete the proof of Property (ii), $\pm[\frac{1}{2}b(\mathbf{y} \cdot \mathbf{k})^2 + p_0(\mathbf{y} \cdot \mathbf{k})]\mathbf{k} \cdot \text{adj}_2 \mathbf{A}$ is added to the last term in (4.6). Using (3.13)-(3.14), we find

$$f_P(\mathbf{u}, \mathbf{x}, \mathbf{A}) - f_P(\mathbf{u}, \mathbf{y}, \mathbf{B}) = I_1 + I_2 + I_3 + I_4, \quad (4.8)$$

where

$$\begin{aligned} I_1 &= -\frac{1}{2}b \left[(\mathbf{x} \cdot \mathbf{k})^2 - (\mathbf{y} \cdot \mathbf{k})^2 \right] \mathbf{k} \cdot \text{adj}_2 \mathbf{A}, \\ I_2 &= -p_0 [(\mathbf{x} \cdot \mathbf{k}) - (\mathbf{y} \cdot \mathbf{k})] \mathbf{k} \cdot \text{adj}_2 \mathbf{A}, \\ I_3 &= -\frac{1}{2}b \left[(\mathbf{y} \cdot \mathbf{k})^2 \right] \mathbf{k} \cdot (\text{adj}_2 \mathbf{A} - \text{adj}_2 \mathbf{B}), \end{aligned}$$

$$I_4 = -p_0 [\mathbf{y} \cdot \mathbf{k}] \mathbf{k} \cdot (\text{adj}_2 \mathbf{A} - \text{adj}_2 \mathbf{B}).$$

By Young's inequality, we have $3|\mathbf{x}| |\mathbf{A}|^2 \leq |\mathbf{x}|^3 + 2|\mathbf{A}|^3$, and $3|\mathbf{y}| |\mathbf{A}|^2 \leq |\mathbf{y}|^3 + 2|\mathbf{A}|^3$. Using these estimates and Lemma 3 with $\tilde{\beta} = 3$, we find

$$\begin{aligned} |I_1| &\leq \frac{1}{2}b|\mathbf{x} - \mathbf{y}| (|\mathbf{x}| + |\mathbf{y}|) |\text{adj}_2 \mathbf{A}| \\ &\leq \frac{3}{2}b|\mathbf{x} - \mathbf{y}| (|\mathbf{x}| + |\mathbf{y}|) |\mathbf{A}|^2 \\ &\leq \frac{1}{2}b \left(|\mathbf{x}|^3 + |\mathbf{y}|^3 + 4|\mathbf{A}|^3 \right) |\mathbf{x} - \mathbf{y}| \\ &\leq 2b \left(1 + |\mathbf{x}|^3 + |\mathbf{y}|^3 + |\mathbf{A}|^3 + |\mathbf{B}|^3 \right) |\mathbf{x} - \mathbf{y}|. \end{aligned} \quad (4.9)$$

Applying Lemma 3 with $\tilde{\beta} = 3$ and Young's inequality with $3|\mathbf{A}|^2 \leq 1 + 2|\mathbf{A}|^3$, we find

$$\begin{aligned} |I_2| &\leq |p_0| |\mathbf{x} - \mathbf{y}| |\text{adj}_2 \mathbf{A}| \\ &\leq 3|p_0| |\mathbf{x} - \mathbf{y}| |\mathbf{A}|^2 \\ &\leq |p_0| \left(1 + 2|\mathbf{A}|^3 \right) |\mathbf{x} - \mathbf{y}| \\ &\leq 2|p_0| \left(1 + |\mathbf{x}|^3 + |\mathbf{y}|^3 + |\mathbf{A}|^3 + |\mathbf{B}|^3 \right) |\mathbf{x} - \mathbf{y}|. \end{aligned} \quad (4.10)$$

Applying Lemma 3 with $\tilde{\beta} = 3$ and Young's inequality with $3|\mathbf{y}|^2|\mathbf{A}| \leq 2|\mathbf{y}|^3 + |\mathbf{A}|^3$ and $3|\mathbf{y}|^2|\mathbf{B}| \leq 2|\mathbf{y}|^3 + |\mathbf{B}|^3$, we find

$$\begin{aligned} |I_3| &\leq \frac{1}{2}b|\mathbf{y}|^2 |\text{adj}_2 \mathbf{A} - \text{adj}_2 \mathbf{B}| \\ &\leq \frac{3}{2}b|\mathbf{y}|^2 (|\mathbf{A}| + |\mathbf{B}|) |\mathbf{A} - \mathbf{B}| \\ &\leq \frac{1}{2} \left(4|\mathbf{y}|^3 + |\mathbf{A}|^3 + |\mathbf{B}|^3 \right) |\mathbf{A} - \mathbf{B}| \\ &\leq 2b \left(1 + |\mathbf{x}|^3 + |\mathbf{y}|^3 + |\mathbf{A}|^3 + |\mathbf{B}|^3 \right) |\mathbf{A} - \mathbf{B}|. \end{aligned} \quad (4.11)$$

Applying Lemma 3 with $\tilde{\beta} = 3$ and the estimates $|\mathbf{y}| |\mathbf{A}| \leq \frac{1}{3} + \frac{2}{3}|\mathbf{y}|^{3/2}|\mathbf{A}|^{3/2} \leq \frac{1}{3}(1 + |\mathbf{y}|^3 + |\mathbf{A}|^3)$ leads to

$$\begin{aligned} |I_4| &\leq |p_0| |\mathbf{y}| |\text{adj}_2 \mathbf{A} - \text{adj}_2 \mathbf{B}| \\ &\leq 3|p_0| |\mathbf{y}| (|\mathbf{A}| + |\mathbf{B}|) |\mathbf{A} - \mathbf{B}| \\ &\leq |p_0| \left(2 + 2|\mathbf{y}|^3 + |\mathbf{A}|^3 + |\mathbf{B}|^3 \right) |\mathbf{A} - \mathbf{B}| \\ &\leq 2|p_0| \left(1 + |\mathbf{x}|^3 + |\mathbf{y}|^3 + |\mathbf{A}|^3 + |\mathbf{B}|^3 \right) |\mathbf{A} - \mathbf{B}|. \end{aligned} \quad (4.12)$$

Combining (4.9)-(4.12), we find

$$\begin{aligned} &|f_P(\mathbf{u}, \mathbf{x}, \mathbf{A}) - f_P(\mathbf{u}, \mathbf{y}, \mathbf{B})| \\ &\leq 2(b + |p_0|) \left(1 + |\mathbf{x}|^3 + |\mathbf{y}|^3 + |\mathbf{A}|^3 + |\mathbf{B}|^3 \right) (|\mathbf{x} - \mathbf{y}| + |\mathbf{A} - \mathbf{B}|). \end{aligned} \quad (4.13)$$

Combining (4.6), (4.7), and (4.13), we see that Property (ii) follows with $\beta = 2 \max\{\beta_1, 2(b + |p_0|)\}$.

Since all of the forces are conservative, equilibrium is achieved at a minimum of the energy functional over the class of functions $X_{\mathbf{g}}$. The constant ρ_1 serves only to increase $W_f^* + f_P$ by a constant, so the minimizer of $W_f^* + f_P$ is the same as the minimizer of $W_f^* + f_P + \rho_1$. We state two existence results for the equilibrium shape of an inflated balloon.

Theorem 1 *Closed balloon system. If $|\mathbf{x}| \leq R$, then*

$$(P_{\mathbf{g}(\omega_0)}) \quad \inf \left\{ I(\mathbf{x}) = \int_{\Omega} f_T^*(\mathbf{u}, \mathbf{x}, \nabla \mathbf{x}) \, dA \mid \mathbf{x} \in X_{\mathbf{g}(\omega_0)} \right\}$$

admits at least one solution.

Since we can always find an $\mathbf{x} \in \mathbf{x}_0 + W_0^{1,4}(\Omega; \mathbb{R}^3)$ parameterizing a spherical cap, we know that $\mathcal{D}_{\mathbf{g}(\omega_0)}$ is nonempty. In order to complete the proof, we need to show that f_T^* is quasiconvex and verify H1 (i)-(iii) in Theorem A.1. Lemma 5 shows that f_T^* is quasiconvex and satisfies H1 (i)-(ii) if $|\mathbf{x}| \leq R$. H1 (iii) is satisfied because f_T^* is independent of \mathbf{u} and so $\eta \equiv 0$. Lemma 4 establishes that $X_{\mathbf{g}(\omega_0)}$ is closed. It follows that $(P_{\mathbf{g}(\omega_0)})$ has at least one solution.

Remark 6 Eq. (1.1) guarantees that the values of b and ω_0 are sufficient to lift the balloon system. If $b = b_d$ and $\omega_0 = \omega_{0,d}$ then the balloon envelope is fully deployed, and we are justified in ignoring the contribution of the film weight in the stress analysis.

Remark 7 In general, one should not expect a unique solution of $(P_{\mathbf{g}(\omega_0)})$, especially if the balloon is not fully inflated. For example, if the lift generated by the gas bubble is not large enough to lift the balloon or the gas is compressed sufficiently (i.e., $\omega_0 < \omega_{0,d}$), then one expects to find multiple local equilibria with slack regions where a unique equilibrium configuration may not exist. For an ascending large scientific balloon, it is not uncommon to observe balloon shapes with a nearly periodic lobe pattern surrounding the gas bubble. These shapes are characterized by significant regions of excess folded material hanging beneath the gas bubble. Folded material can be handled by introducing constraints in the form covered by Lemma 1 and the theory developed in this paper applies to shapes with a period lobe pattern.

Theorem 2 *Open balloon system. If $|\mathbf{x}| \leq R$, then*

$$(P_{\mathbf{g}}) \quad \inf \left\{ I(\mathbf{x}) = \int_{\Omega} f_T^*(\mathbf{u}, \mathbf{x}, \nabla \mathbf{x}) \, dA \mid \mathbf{x} \in X_{\mathbf{g}} \right\}$$

admits at least one solution.

Description	Variable	Value
Number of gores	n_g	200
Buoyancy (N/m ³)	b	0.068
Tendon weight density (N/m)	w_t	0.094
Film weight density (N/m ²)	w_f	0.344
Payload (N)	L	4000
End-plate diameter (m)	d_1	1.32

Table 1: Shape finding parameters. For pumpkin balloons we assumed $r_B = 0.785$ m and $p_0 = 200$ Pa. For ZPNS balloons, $p_0 = 0$ Pa. Tendon weight and film weight are included in the shape finding process.

Description	Variable	Value
Film Young’s modulus (MPa)	E_f	404.2
Film Poisson ratio	ν_f	0.825
Film thickness (μm)	t	32

Table 2: Mechanical properties of polyethylene film.

Since the subspace $X_{\mathbf{g}}$ is closed by Lemma 1, the proof of Theorem 2 is the same as the proof of Theorem 1 with the space $X_{\mathbf{g}(\omega_0)}$ replaced by $X_{\mathbf{g}}$.

5 Numerical results on strained balloon shapes

In this section, we present numerical solutions of our model. We consider a zero-pressure natural shape design and a pumpkin design. We assume the balloon film is $32\mu\text{m}$ polyethylene and the balloons have no caps. We use the same tendon weight density and a suspended payload of 4000 N for both balloons in shape finding. The specific buoyancy at float is $b = 0.068$ N/m³ and corresponds to an altitude of roughly 35 km. For the pumpkin balloon, $r_B = 0.785$ m and $p_0 = 200$ Pa. See Table 1 for a summary of shape finding parameters that were used. We used mechanical properties that were determined by the Balloon Lab at NASA’s Wallops Flight Facility for 0.8 mil polyethylene film at room temperature (this is comparable to the temperature at float during nominal daylight conditions). For an isotropic three-dimensional material, one can show that Poisson’s ratio is between 0 and 0.5 (see, [13, p. 129]). However, in lab experiments using cylinder tests, one finds that for a thin polyethylene film, Poisson’s ratio is greater than 0.5 (see, e.g., [11]). We extrapolated the findings for 0.8 mil to 1.5 mil film to estimate Young’s modulus for our simulations. Mechanical properties are summarized in Table 2.

Next, we summarize our findings when we numerically solved Problems $(P_{\mathbf{g}})$ and $(P_{\mathbf{g}(\omega_0)})$. In all cases, we assumed a cyclically symmetric shape and so we needed to solve for one-half a gore. We divided a half-gore into three strips with 100 triangles per strip. We used our own finite element

code written in Matlab to compute the energies and constraints as described in Sections 3-5. We then used `fmincon` from Matlab's Optimization ToolBox to solve a constrained minimization problem where f_T^* was the objective function and $\mathbf{g} \leq 0$ were the constraints. Gradients for f_T^* , \mathbf{g} , and the Hessian of f_T^* were computed analytically. When a nonlinear constraint (i.e., volume or tendon constraint) is imposed, we used a “medium-scale” sequential quadratic programming quasi-Newton’s method; when there were only linear constraints, a “large-scale” projected trust-region Newton’s method was used (see, [14] for further details on these algorithms).

We discretized the three-dimensional surface produced by the shape finding process and used this as an initial guess to start the solution process. For each of the scenarios considered, we present plots of the “averaged” principal strains and “averaged” principal stress resultants for each adjacent pair of rectangles in a strip. If a meridional strip has $2M$ triangles (numbered from top to bottom) and $\mu_{2i-1,1}$ and $\mu_{2i,1}$ are the meridional principle stress resultants, then we plot $\frac{1}{2}(\mu_{2i-1,1} + \mu_{2i,1})$ for $i = 1, \dots, M$. Note, the directions for $\mu_{2i-1,1}$ and $\mu_{2i,1}$ need not coincide, but this measure seems to work satisfactorily for summarizing the data. A similar convention is followed for averaging the circumferential stress resultants and the principal strains.

5.1 Zero-pressure natural shape balloon.

We considered two scenarios involving a ZPNS balloon.

- (a) *Closed system* $V(\mathbf{x}) = \omega_0$. In this case, we considered a closed system with a target volume $\omega_0 = 137,023 \text{ m}^3$. The averaged principal strains are plotted in Figure 6(a) and the averaged principal stress resultants are plotted in Figure 6(b). The δ_1 and δ_2 directions corresponds roughly to meridional and circumferential, respectively. We found that the maximum principal strains were less than 0.03%. The meridional stress resultants are plotted in the top graph in Figure 6(b) and increase monotonically from the bottom of the gore to its top. From Figure 6(b), we see that near the top one-third, the film is in a biaxial state and in the middle one-third it is in a uniaxial or near uniaxial state (i.e., $\mu_{2,i} \approx 0$).
- (b) *Open system* $p_0 = 0$. In Section 5.1(b), we considered the same conditions as those in Section 5.1(a), except we dropped the volume constraint and set $p_0 = 0$. The results were nearly identical to those obtained in Section 5.1(a) and for this reason plots were not included. We found that the difference between the volumes in Section 5.1(a) and (b) was less than 10^{-5} m^3 .

In the following, principal strains and stress resultants are to be interpreted as ‘averaged’ principal strains and ‘averaged’ principal stress resultants, respectively.

5.2 Pumpkin balloon without tendons.

To get a sense of the important role that tendons play in a pumpkin balloon, we computed a solution for a pumpkin balloon without tendons. Since it was clear that a single layer of $32\ \mu\text{m}$ film was not sufficiently strong, we quadrupled the thickness for this numerical experiment. From Figure 7(a) we see that the strains are nearly 7.0% and the principal stress resultants are quite large (a maximum of 8 kN/m). It is interesting to note that near the ends, the deformed gore is in a state of biaxial tension, where in the middle of the gore the tension is uniaxial and parallel to the gore length. In reality, the film is a viscoelastic material and under the right conditions may be able to maintain the integrity of the gas barrier at such a high strain. However, the peaks in Figure 7 suggest this loading scenario should be avoided.

5.3 Pumpkin balloon with tendons.

In this case, we considered a single layer of $32\ \mu\text{m}$ polyethylene film and added inextensible tendons via a constraint (i.e., (3.44)). In Figures 8(a)-(b), we present the principal strains and principal stress resultants. We see that when tendons are added, the maximum principal strains are reduced from 7.0% in Section 5.2 to 1.5%. The maximum principal stress resultants are reduced from 8 kN/m in Section 5.2 to 225 N/m. It is interesting to note from the plot of the circumferential stress resultants (bottom graph of Figure 8(b)), the film is in a state of biaxial stress along the center of the gore. But near the equator and the sub-tropic regions, as one gets closer to the tendon, the film is in a uniaxial state. This makes sense because one would expect there to be wrinkling in these locations.

5.4 Pumpkin balloon with shortened tendons

In Figures 9(a)-(b), we plot the principal strains and principal stress resultants when shortened tendons are utilized. Basically, we reduced the tendon length in Section 5.3 by 2%. Overall, we see that the principal strains and principal stress resultants are reduced. However, the maximum principal strains and principal stress resultants are not reduced by a significant amount. Comparing Figure 8(b) and Figure 9(b), we see more wrinkling in Figure 9(b), especially in the area adjacent to the tendons.

While there are many other factors that go into the design of a gore, a balloon of the type discussed in Section 5.4 is not very efficient. Ideally, one would like to have the gore uniformly loaded. The presence of wrinkles in the fully inflated shape suggests that there is excess material that is doing little to carry its share of the load. Furthermore, it has been demonstrated that too much tendon shortening can be detrimental, leading to instability in the strained cyclically symmetric float shape and impeding proper deployment (see, [5]-[7]).

6 Conclusions

Motivated by the problem of a large scientific balloon at float altitude, we presented a mathematical model for a strained inflated wrinkled membrane loaded by hydrostatic pressure and constrained by tendons. We assumed the balloon is constructed of a thin linearly elastic isotropic material. Load tendons are included through the use of constraints. Using direct methods in the calculus of variations we established rigorous existence theorems under general conditions. We computed numerical solutions based on our model and estimated the principal strains and principal stress resultants under nominal loading conditions at float altitude. Our theoretical results establish a solid foundation for our mathematical model and affirms the use of numerical computations to estimate film stress resultants, information that is valuable to the balloon designer. An efficient balloon design keeps weight to a minimum, but the balloon must be of sufficient strength to operate safely over its service life. Analytical and computational tools are demonstrated here that can help the balloon designer balance the competing factors of a stronger, albeit heavier balloon versus a lighter more efficient one.

Acknowledgement

The first two authors were supported by NASA Grant NAG5-5353.

References

- [1] ANON.: *Research Development in the Field of High Altitude Plastic Balloons*, NONR-710(01a) Reports, Department of Physics, University of Minnesota, Minneapolis, Minnesota, 1951-1956.
- [2] S. S. ANTMAN: *Nonlinear Problems of Elasticity*, Springer-Verlag, New York, 1995.
- [3] T. AUBIN: *Nonlinear analysis on Manifolds. Monge-Ampère Equations*, Springer-Verlag, New York, 1982.

- [4] F. E. BAGINSKI: *On the design and analysis of inflated membranes: natural shape and pumpkin shaped balloons*, SIAM J. Appl. Math. **65** No. 3 838-857 (2005).
- [5] F. BAGINSKI, K. BRAKKE & W. W. SCHUR: *Stability of cyclically symmetric strained pumpkin balloon configurations and the formation of undesired equilibria*, accepted for publication in the AIAA Journal of Aircraft.
- [6] F. BAGINSKI, K. BRAKKE & W. W. SCHUR: *Unstable cyclically symmetric and stable asymmetric configurations of a pumpkin balloon*, accepted for publication in the AIAA Journal of Aircraft.
- [7] F. BAGINSKI, K. BRAKKE & W. W. SCHUR: *Cleft formation in pumpkin balloons*, Adv. Space Res., **37** 2070-2081 (2006).
- [8] F. BAGINSKI & W. W. SCHUR: *Undesired equilibria of self-deploying pneumatic envelopes*, AIAA Journal of Aircraft, **42** No. 6 1639-1642 (2005).
- [9] F. BAGINSKI & W. SCHUR: *Structural analysis of pneumatic envelopes: A variational formulation and optimization-based solution process*, AIAA Journal, **41** No. 2 304-311 (2003).
- [10] J. M. BALL: *Convexity conditions and existence theorems in nonlinear elasticity*, Arch. Ration. Mech. Anal. **63** 337-403 (1977).
- [11] J. BLANDINO, J. STERLING, F. BAGINSKI, E. STEADMAN, J. T. BLACK & R. PAPPA: *Optical strain measurement of an inflated cylinder using photogrammetry with application to scientific balloons*, AIAA-2004-1500, 45th AIAA/ASME/ASCE/AHS/ASC Structures, Structural Dynamics, and Materials Conference, 19-22 April 2004, Palm Springs, CA.
- [12] P. G. CIARLET: *Mathematical Elasticity Volume III: Theory of Shells*, North-Holland, New York, 2000.
- [13] P. G. CIARLET: *Mathematical Elasticity Volume I: Three-Dimensional Elasticity*, North-Holland, New York, 1988.
- [14] T. COLEMAN, M. A. BRANCH & A. GRACE: *Optimization ToolBox. User Guide*, The MathWorks, Natick, MA, 1999.
- [15] W. COLLIER: *Estimating stresses in a partially inflated high altitude balloon using a relaxed energy approach*, **61** No. 1 17-40 (2003).

- [16] B. DACOROGNA: *Direct Methods in the Calculus of Variations*, Springer-Verlag, New York, 1989.
- [17] M. P. DO CARMO: *Differential Geometry of Curves and Surfaces*, Prentice-Hall, Englewood Cliffs, NJ, 1976.
- [18] L. C. EVANS: *Partial Differential Equations*, Graduate Studies in Mathematics, Vol. 19, American Mathematical Society, 2002.
- [19] D. FISHER: Configuration dependent pressure potentials, *Journal of Elasticity*, **19** (1988) 77-84.
- [20] D. GILBARG & N. S. TRUDINGER: *Elliptic Partial Differential Equations of Second Order*, Springer-Verlag, Berlin, 1983.
- [21] W. V. JONES: Evolution of Scientific Ballooning, 29th International Cosmic Ray Conference, Pune **10** 173-184 (2004).
- [22] W. V. JONES: Pioneering space research with balloons, COSPAR 2006-A-03074, 36th COSPAR Scientific Assembly, 16-23 July 2006, Beijing, China.
- [23] A. LIBAI & J. G. SIMMONDS: *The nonlinear theory of elastic shells*, 2nd Edition, Cambridge University Press, New York, 1998.
- [24] A. C. PIPKIN: *Relaxed energy densities for large deformations of membranes*, *IMA Journal of Applied Mathematics*, **52** 297-308 (1994).
- [25] J. H. SMALLEY: *Development of the e-balloon*, AFCRL-70-0543, National Center for Atmospheric Research, Boulder, Colorado, June 1970.
- [26] D. J. STEIGMAN & A. C. PIPKIN: *Axisymmetric tension fields*, *ZAMP*, **40** 526-542 (1989).
- [27] M. STEIN & J. M. HEDGEPTH: *Analysis of partially wrinkled membranes*, NASA TN D-813, 1961.
- [28] G. I. TAYLOR: *On the stability of parachutes*, in *The Scientific Papers of Sir G. I. Taylor*, Vol. III, ed. G. K. Batchelor, Cambridge University Press, 1963.

A Direct methods in the calculus of variations

For the convenience of the reader, we record two results by Dacorogna.

Lemma A.1 *Dacorogna [16, Lemma 2.2, p. 156] Let $f : \mathbb{R}^n \rightarrow \mathbb{R}$ be convex in each variable and let*

$$|f(x)| \leq \alpha(1 + |x|^p)$$

for every $x \in \mathbb{R}^n$ and where $\alpha \geq 0, p \geq 1$. Then there exists $\beta \geq 0$ such that

$$|f(x) - f(y)| \leq \beta(1 + |x|^{p-1} + |y|^{p-1})|x - y|$$

for every $x, y \in \mathbb{R}^n$.

Theorem A.1 *Dacorogna [16, Theorem 2.9, p. 180] Let $\Omega \subset \mathbb{R}^n$ be a bounded open set. Let $f : \Omega \times \mathbb{R}^m \times \mathbb{R}^{nm} \rightarrow \mathbb{R}$ be continuous and quasiconvex and satisfying*

(i) $\gamma|\mathbf{A}|^p \leq f(\mathbf{u}, \mathbf{x}, \mathbf{A}) \leq \delta(1 + |\mathbf{x}|^p + |\mathbf{A}|^p);$

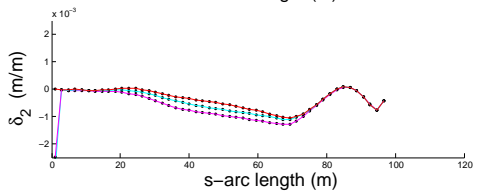
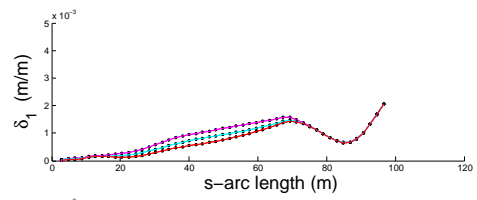
(ii) $|f(\mathbf{u}, \mathbf{x}, \mathbf{A}) - f(\mathbf{u}, \mathbf{y}, \mathbf{B})| \leq \beta(1 + |\mathbf{x}|^{p-1} + |\mathbf{y}|^{p-1} + |\mathbf{A}|^{p-1} + |\mathbf{B}|^{p-1})(|\mathbf{x} - \mathbf{y}| + |\mathbf{A} - \mathbf{B}|);$

(iii) $|f(\mathbf{u}, \mathbf{x}, \mathbf{A}) - f(\mathbf{v}, \mathbf{x}, \mathbf{A})| \leq \eta(|\mathbf{u} - \mathbf{v}|)(1 + |\mathbf{x}|^p + |\mathbf{A}|^p)$ where η is a continuous increasing function with $\eta(0) = 0$ and $p > 1, \alpha, \beta, \gamma > 0$ are constants.

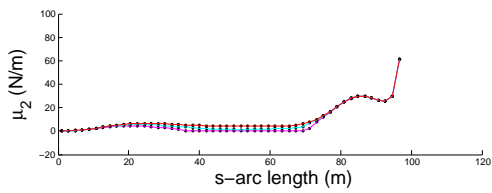
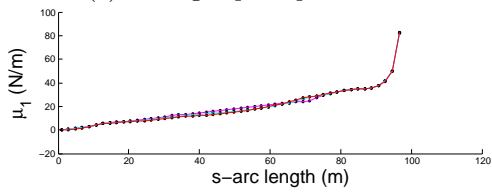
Let

$$(P) \quad \inf \left\{ I(\mathbf{x}) = \int_{\Omega} f(\mathbf{u}, \mathbf{x}(\mathbf{u}), \nabla \mathbf{x}(\mathbf{u})) \, dA : \mathbf{x} \in \mathbf{x}_0 + W_0^{1,p}(\Omega; \mathbb{R}^m) \right\} \quad (1.1)$$

then (P) admits at least one solution.

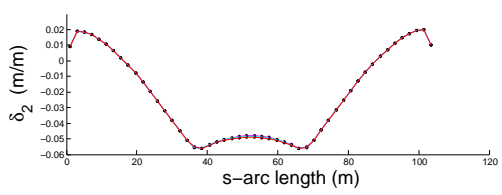
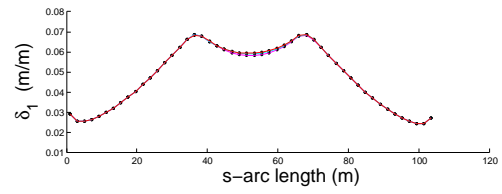


(a) Averaged principal strains

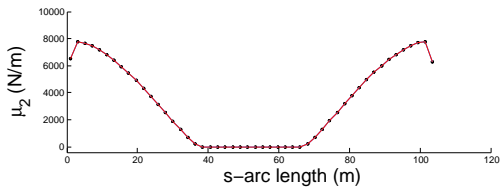
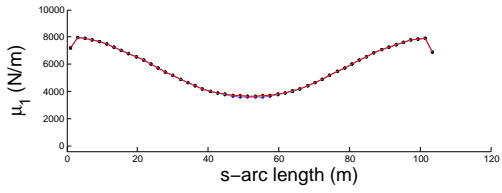


(b) Averaged principal stress resultants

Figure 6: Zero-pressure natural shape balloon with tendon and volume constraints.



(a) Averaged principal strains



(b) Averaged principal stress resultants

Figure 7: Pumpkin balloon without tendon constraints and nominal thickness quadrupled.

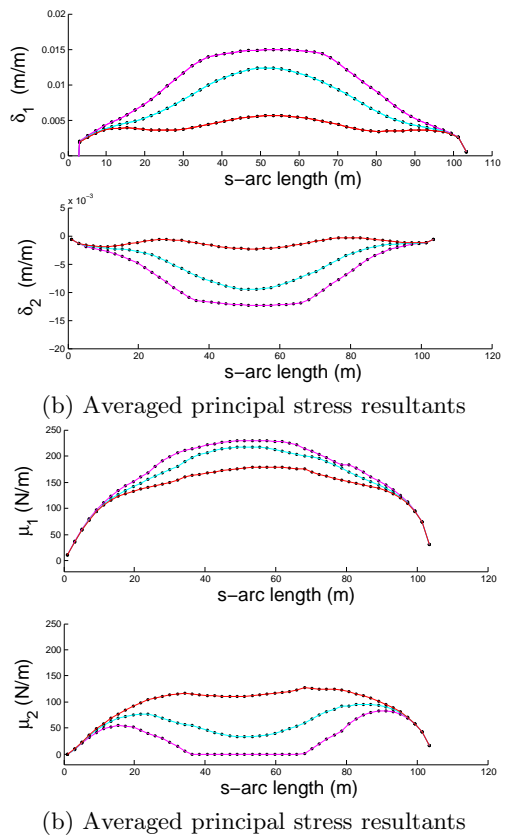


Figure 8: Pumpkin balloon with tendon constraints.

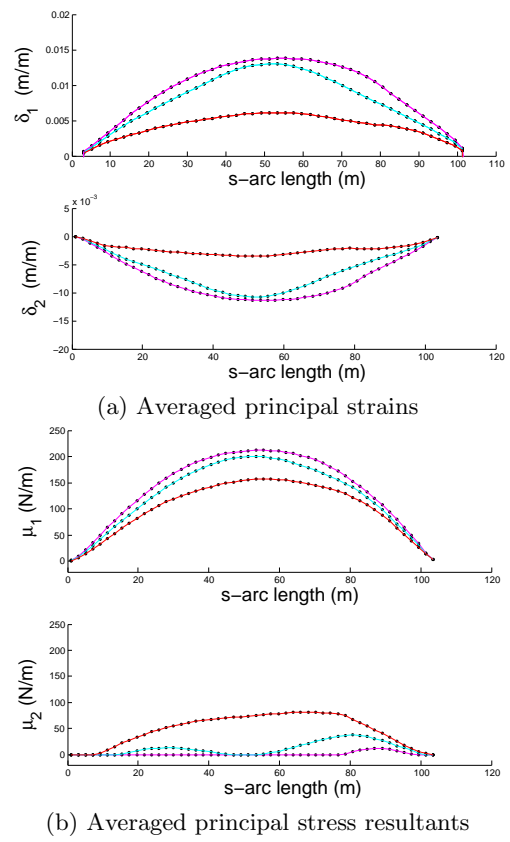


Figure 9: Pumpkin balloon with tendons shortened by 2%.